

Chemical abundances of the Galactic H II region NGC 3576 derived from VLT echelle spectrophotometry¹

Jorge García-Rojas

Instituto de Astrofísica de Canarias, E-38200, La Laguna, Tenerife, Spain

jogarcia@ll.iac.es

César Esteban

Instituto de Astrofísica de Canarias, E-38200, La Laguna, Tenerife, Spain

cel@ll.iac.es

Manuel Peimbert

Instituto de Astronomía, UNAM, Apdo. Postal 70-264, México 04510 D.F., Mexico

peimbert@astroscu.unam.mx

Mónica Rodríguez

*Instituto Nacional de Astrofísica, Óptica y Electrónica, Apdo. Postal 51 y 216, 72000
Puebla, Mexico*

mrodri@inaoep.mx

María Teresa Ruiz

*Departamento de Astronomía, Universidad de Chile, Casilla Postal 36D, Santiago de
Chile, Chile*

mtruiz@das.uchile.cl

and

Antonio Peimbert

Instituto de Astronomía, UNAM, Apdo. Postal 70-264, México 04510 D.F., Mexico

antonio@astroscu.unam.mx

¹Based on observations collected at the European Southern Observatory, Chile, proposal number ESO 68.C-0149(A).

ABSTRACT

We present echelle spectrophotometry of the Galactic H II region NGC 3576. The data have been taken with the VLT UVES echelle spectrograph in the 3100 to 10400 Å range. We have measured the intensities of 458 emission lines, 344 are permitted lines of H⁰, He⁰, C⁺, N⁰, N⁺, N⁺⁺, O⁰, O⁺, Ne⁺, S⁺⁺, Si⁰, Si⁺, Ar⁰ and Ar⁺; some of them are produced by recombination and others mainly by fluorescence. Electron temperatures and densities have been determined using different continuum and line intensity ratios. We have derived He⁺, C⁺⁺, O⁺, O⁺⁺ and Ne⁺⁺ ionic abundances from pure recombination lines. We have also derived abundances from collisionally excited lines for a large number of ions of different elements. Remarkably consistent estimations of t^2 have been obtained by comparing Balmer and Paschen to [O III] temperatures, and O⁺⁺ and Ne⁺⁺ ionic abundances obtained from collisionally excited and recombination lines. The chemical composition of NGC 3576 is compared with those of other Galactic H II regions and with the one from the Sun. A first approach to the gas-phase Galactic radial abundance gradient of C as well as of the C/O ratio has been made.

Subject headings: line:identification. ISM:abundances—H II regions. individual:(NGC 3576)

1. Introduction

NGC 3576 —also known as Gum38a— comprises the western part of the RCW 57 complex (Rodgers, Campbell, & Whiteoak 1960) and corresponds to a bright knot embedded in a large system of diffuse emission gas filaments (Girardi et al. 1997). This knot is one of the most luminous Galactic H II regions in the infrared (Figuêredo et al. 2002). It was thought that most of the ionization of NGC 3576 is due to two O stars (HD 97319 and HD 97484) and two B stars (HD 974999 and CPD–60°2641) which are the main visual components of the OB association (Humphreys 1978); but recent infrared observations suggest that the main ionizing sources of this H II region are behind heavily obscuring clouds (Boreiko & Betz 1997; Figuêredo et al. 2002). It is located in Carina at a distance of 2.7 kpc (Russeil 2003) and at a Galactocentric distance of 7.4 kpc (assuming a Galactocentric solar distance of 8.0 kpc).

Previous abundance determinations for NGC 3576 are those by Girardi et al. (1997), based on the analysis of collisionally excited lines (hereafter CELs); Tsamis et al. (2003)

based on CELs and some recombination lines (hereafter RLs) of C^{++} and O^{++} ; and Simpson et al. (1995) based on far-infrared data and photoionization models.

The temperature fluctuations problem (Peimbert 1967) is, nowadays, a much-discussed topic in astrophysics of gaseous nebulae (Liu 2002, 2003; Esteban 2002; Torres-Peimbert & Peimbert 2003). Traditionally, the abundance studies for H II regions have been based on determinations from CELs, which are strongly dependent on the temperature variations over the observed volume of the nebula. Alternatively, RLs are almost independent of such variations and are, in principle, more precise indicators of the true chemical abundances of the nebula. Several authors have obtained O^{++}/H^+ from O II recombination line intensities for the brightest H II regions of the Galaxy (Peimbert, Storey & Torres-Peimbert 1993; Esteban et al. 1998, hereafter EPTE; Esteban et al. 1999a, hereafter EPTGR; Esteban et al. 1999b; Tsamis et al. 2003), for extragalactic H II regions (Esteban et al. 2002; Peimbert 2003; Tsamis et al. 2003) and for planetary nebulae (Liu et al. 2000, 2001; Ruiz et al. 2003; Peimbert et al. 2004), and all of them have found that the abundance determinations from RLs are systematically larger than those obtained using CELs. The CEL abundances depend strongly on the adopted temperature while the RL abundances are almost independent of it. In the presence of temperature inhomogeneities the temperature derived from the [O III] diagnostic lines, $T_e(O\ III)$, is considerably higher than the average one and than those temperatures derived from the Balmer and Paschen continua. For H II regions the differences in both the abundances derived from CELs and RLs and the temperatures derived from CELs and recombination processes, can be consistently accounted for by assuming a t^2 (mean square temperature variation over the observed volume) in the range 0.020–0.044.

O’Dell et al. (2003, see also Rubin et al. 2003) have used a different method to show that there are temperature inhomogeneities in H II regions: these authors have determined the columnar temperature along 1.5×10^6 lines of sight in the Orion nebula, the distribution of temperatures of their sample supports the t^2 values derived from other methods. The origin of temperature fluctuations is still controversial and a serious challenge to our knowledge of the physics and structure of ionized nebulae.

We have taken long-exposure high-spectral-resolution spectra with the VLT UVES echelle spectrograph to obtain accurate measurements of very faint permitted lines of heavy element ions in NGC 3576. We have determined the physical conditions and the chemical abundances of NGC 3576 with high accuracy, including important improvements over previous determinations. We have considered C^{++} and O^{++} abundances obtained from several permitted lines of C II and O II, avoiding the problems of line blending, including several 3d-4f transitions which are very useful for abundance determinations because they are free of optical depth effects (Liu et al. 1995 and references therein). We have also derived O^+ and

Ne^{++} abundances from RLs for the first time in this nebula. We have computed t^2 values from the determination of the Balmer and Paschen temperatures, which coincide with the t^2 that produces the agreement between the ionic abundances obtained from CELs and RLs. Finally, we have determined helium abundances taking into account a large number of singlet lines of He I.

In §§ 2 and 3 we describe the observations and the data reduction procedure. In § 4 we obtain temperatures and densities using several diagnostic ratios; also, in this section, we determine t^2 from different line intensity ratios and temperature determinations. In § 5 we briefly analyze the recombination spectra of He I and derive the He^+/H^+ ratio. In § 6 ionic abundances are determined based on RLs, as well as on CELs. In § 7 the total abundances are determined. In §§ 8 and 9 we present the discussion and the conclusions, respectively.

2. Observations and Data Reduction

The observations were made on 2002 March 11 with the Ultraviolet Visual Echelle Spectrograph, UVES (D’Odorico et al. 2000), at the VLT Kueyen Telescope in Cerro Paranal Observatory (Chile). We used the standard settings in both the red and blue arms of the spectrograph, covering the region from 3100 to 10400 Å. The log of the observations is presented in Table 1.

The wavelength regions 5783–5830 Å and 8540–8650 Å were not observed due to a gap between the two CCDs used in the red arm. There are also five small gaps that were not observed, 9608–9612 Å, 9761–9767 Å, 9918–9927 Å, 10080–10093 Å and 10249–10264 Å, because the five redmost orders did not fit completely within the CCD. We took long and short exposure spectra to check for possible saturation effects.

The slit was oriented east-west and the atmospheric dispersion corrector (ADC) was used to keep the same observed region within the slit regardless of the air mass value. The slit width was set to 3.0'' and the slit length was set to 10'' in the blue arm and to 12'' in the red arm; the slit width was chosen to maximize the S/N ratio of the emission lines and to maintain the required resolution to separate most of the weak lines needed for this project. The effective resolution for the NGC 3576 lines at a given wavelength is approximately $\Delta\lambda \sim \lambda/8800$. The center of the slit was placed 65'' west and 24 '' north of HD 97499, covering the brightest region of NGC 3576. The reductions were made for an area of 3''×8.25'' in the blue arm (B1 and B2), 3''×10.1'' in the red arm (R1) and 3''×9.5'' in the R2 configuration of the red arm. These areas were chosen in order to maximize the S/N ratio of the emission lines. A test was made to confirm that line fluxes were not significantly

affected by the different areas chosen in each spectral range.

The spectra were reduced using the IRAF² echelle reduction package, following the standard procedure of bias subtraction, aperture extraction, flatfielding, wavelength calibration and flux calibration. The standard star EG 247 was observed for flux calibration.

3. Line Intensities and Reddening Correction

Line intensities were measured integrating all the flux in the line between two given limits and over a local continuum estimated by eye. In the cases of line blending, a multiple Voigt profile fit procedure was applied to obtain the line flux of each individual line. Most of these measurements were made with the SPLOT routine of the IRAF package. In some cases of very tight blends or blends with very bright telluric lines the analysis was performed via Gaussian fitting making use of the Starlink DIPSO software (Howard & Murray 1990).

Table 2 presents the emission line intensities of NGC 3576. The first and fourth columns include the adopted laboratory wavelength, λ_0 , and the observed wavelength in the heliocentric framework, λ . The second and third columns include the ion and the multiplet number, or series for each line. The fifth and sixth columns include the observed flux relative to $H\beta$, $F(\lambda)$, and the flux corrected for reddening relative to $H\beta$, $I(\lambda)$. The seventh column includes the fractional error (1σ) in the line intensities (see § 3.1).

A total of 458 emission lines were measured; of them 344 are permitted, 108 are forbidden and 2 are semiforbidden (see Table 2). Some [N I] and [O I] lines were detected, but they are blended with telluric lines, making impossible their measurement. Several other lines were strongly affected by atmospheric features in absorption or by internal reflections by charge transfer in the CCD, rendering their intensities unreliable. Also, 29 lines are dubious identifications and 4 emission lines could not be identified in any of the available references. Those lines are indicated in Table 2.

The identification and adopted laboratory wavelengths of the lines were obtained following previous identifications in the Orion Nebula by EPTE, Baldwin et al. (2000) and Osterbrock, Tran, & Veilleux (1992); we also used the compilations of atomic data by Moore (1945, 1993), Wiese, Smith, & Glennon (1966), the line catalogue for gaseous nebulae of Feklistova et al. (1994), the catalogue of Péquignot & Baluteau (1988) for He I lines and the papers of EPTGR on M8, Esteban et al. (1999b) on M17 and Liu et al. (2000, 2001) on spectrophotometry of the planetary nebulae NGC 6153, M 1-42 and M 2-36. Also, we have

²IRAF is distributed by NOAO, which is operated by AURA, under cooperative agreement with NSF.

used an interactive source of nebular data: The Atomic Line List v2.04³, directly or through the *EMILI*⁴ code (Sharpee et al. 2003)

Following Girardi et al. (1997) we have assumed the extinction law of Savage & Mathis (1979) with $R_v=3.1$. A reddening coefficient of $C(H\beta)=1.40\pm0.07$ dex was determined by fitting the observed $I(\text{H Balmer lines})/I(H\beta)$ ratios (from H16 to $H\beta$) and $I(\text{H Paschen lines})/I(H\beta)$ (from P22 to P7), to the theoretical ones computed by Storey & Hummer (1995) for $T_e = 9000$ K and $N_e = 1000 \text{ cm}^{-3}$ (see below). H I lines affected by blends or atmospheric absorption were not considered.

3.1. Errors

The observational errors associated with the line intensities have been determined taking into account two sources of uncertainty: statistical errors in the line flux measurements and $C(H\beta)$ uncertainty. It has not been possible to determine the systematic error of the flux calibration because we used a single standard star (EG 274). However, the comparison between observed and theoretical Balmer and Paschen line ratios of the brightest –and no sky-affected– lines show that the average differences are below 3%. Moreover, in a future paper (Esteban et al., in preparation), we compare the echelle observations of EPTE with new VLT data for the same zone of the Orion nebula. These VLT data have been flux calibrated in identical form than our observations of NGC 3576 and do not show any systematical differences in the emission line ratios in common with EPTE, which differ typically not more than 3%. Therefore, we can conclude that the flux calibration of the data presented in the present paper is confident, and it is not a source of significant systematical uncertainties.

The method developed to determine the line uncertainties consist of the following steps: firstly, the spectral ranges with the same exposure time (B1 and R1; B2 and R2) are grouped, then in each of these ranges several lines covering all the intensity ranges are chosen and the statistical errors are computed using the IRAF SPLOT task. Error propagation theory and a logarithmic interpolation of $F(\lambda)/F(H\beta)$ vs. $\sigma(F(\lambda)/F(H\beta))$ are used to determine $\sigma(F(\lambda)/F(H\beta))$ for each line. Taking into account the uncertainties in the determination of $C(H\beta)$ and error propagation, the final percentile errors (1σ) of the $I(\lambda)/I(H\beta)$ ratios are computed and presented in column 7 of Table 2. Colons indicate errors higher than 40 %.

³webpage at: <http://www.pa.uky.edu/~peter/atomic/>

⁴webpage at: <http://www.pa.msu.edu/astro/software/emili/>

4. Physical Conditions

4.1. Temperatures and Densities

The large number of emission lines identified and measured in the spectra allows us the derivation of physical conditions using different line ratios. The temperatures and densities are presented in Table 3. Most of the determinations were carried out with the IRAF task TEMDEN of the package NEBULAR, based in the FIVEL program developed by De Robertis, Dufour, & Hunt (1987) and improved by Shaw & Dufour (1995).

A representative initial T_e of 10000 K was assumed in order to derive $N_e(\text{O II})$, $N_e(\text{S II})$, $N_e(\text{Cl III})$ and $N_e(\text{Ar IV})$. On the other hand, we have derived the $[\text{Fe III}]$ density from the intensity of 14 lines, that seem not to be affected by line blending, together with the computations of Rodríguez (2002). The computed value is very consistent with the densities derived from $[\text{Cl III}]$ and $[\text{Ar IV}]$ lines. From Table 3 it can be seen that all diagnostic ratios are in good agreement, except the densities obtained from $[\text{O II}]$ and $[\text{S II}]$, which give lower values than the other indicators.

We have derived $N_e(\text{O II})$ using the classical ratio $\lambda 3726/\lambda 3729$. In spite of the low critical density of the highest level of the $\lambda 3729$ transition, this ratio does not saturate in NGC 3576, but with this density we obtained a value of $T_e(\text{O II})=10800$ K which is too high if compared with $T_e(\text{S II})$ and $T_e(\text{N II})$. Due to the extreme sensitivity of $T_e(\text{O II})$ with the adopted density, we have decided to use the $\lambda\lambda 3726+3729/\lambda\lambda 7320+7330$ ratio to derive a new $N_e(\text{O II})$, because the abundances obtained with the different individual lines of $[\text{O II}]$ assuming this density and $T_e(\text{N II})$ are more consistent than those obtained with the density derived from the usual ratio. It is not the aim of this work to solve this problem but it could be due to several reasons including errors in the O II atomic data and the uncertainty in the contribution of recombination to the excitation of the auroral lines. To obtain $N_e(\text{O II})$ it is necessary to subtract the contribution to $\lambda\lambda 7320+7330$ due to recombinations; Liu et al. (2000) find that the contribution to the intensities of the $[\text{O II}]$ $\lambda\lambda$ 7319, 7320, 7331, and 7332 lines due to recombination can be fitted in the range $0.5 \leq T/10^4 \leq 1.0$ by:

$$\frac{I_R(7320 + 7330)}{I(\text{H}\beta)} = 9.36 \times (T_4)^{0.44} \times \frac{\text{O}^{++}}{\text{H}^+}, \quad (1)$$

where $T_4=T/10^4$. With this equation we estimate a contribution of approximately 6% to the observed line intensities.

A weighted average of $N_e(\text{O II})$, $N_e(\text{Fe III})$, $N_e(\text{Cl III})$ and $N_e(\text{Ar IV})$ was then used to derive $T_e(\text{N II})$, $T_e(\text{O III})$, $T_e(\text{Ar III})$ and $T_e(\text{S III})$, and iterated until convergence. So, for all the species except for S^+ the adopted value for the density is: $N_e=2800 \pm 400 \text{ cm}^{-3}$.

For S⁺ we have adopted $N_e(\text{S II})=1300_{-300}^{+500} \text{ cm}^{-3}$, because this ion has the lowest ionization potential of all the species studied. The $T_e(\text{S II})$ derived making use of this density is much more consistent with temperatures derived using other diagnostic ratios than that derived with $N_e=2800 \text{ cm}^{-3}$, which gives a temperature 2000 K lower.

Liu et al. (2000) determined that the contribution to the intensity of the $\lambda 5755$ [N II] line due to recombination can be estimated from:

$$\frac{I_R(5755)}{I(\text{H}\beta)} = 3.19 \times (T_4)^{0.30} \times \frac{N^{++}}{H^+}, \quad (2)$$

in the range $0.5 \leq T/10^4 \leq 2.0$. We have obtained a contribution of recombination of about 7.5%, that represents a decrease of more than 200 K in the temperature determination.

Finally, considering the similarity of the temperature determinations based on CELs, an average of [O III] and [N II] temperatures was adopted for NGC 3576, assuming a 1-zone ionization scheme. This is because these diagnostic temperatures are the usually adopted ones to characterize high and low ionization zones respectively, and because in our case they are coincident. We obtain a representative value of $T_e=8500 \pm 150$ K. $T_e(\text{S II})$ and $T_e(\text{Ar III})$ temperatures are absolutely consistent with the adopted temperature and do not affect to the average. We have not included $T_e(\text{S III})$ because this is the most discrepant value.

The Balmer continuum temperature was determined following the equation by Liu et al. (2001):

$$T(\text{Bac}) = 368 \times (1 + 0.259y^+ + 3.409y^{++}) \left(\frac{\text{Bac}}{\text{H11}} \right)^{-3/2} \text{ K}; \quad (3)$$

where y^+ and y^{++} are the He^+/H^+ and $\text{He}^{++}/\text{H}^+$ ratios respectively, and Bac is the value of the discontinuity of the balmer jump in $\text{erg cm}^{-2} \text{ s}^{-1} \text{ \AA}^{-1}$. A power-law fit to the relation between $I_c(\text{Bac})/I(\text{H}n)$ and T_e for $3 \leq n \leq 20$ gives the same result as the method mentioned above, but higher uncertainties due to the statistical dispersion. The Paschen continuum temperature was derived fitting the relation between $I_c(\text{Pac})/I(\text{P}n)$ and T_e for $7 \leq n \leq 25$. The emissivities as a function of the electron temperature for the nebular continuum and the H I Balmer and Paschen lines were taken from Brown & Mathews (1970) and Storey & Hummer (1995) respectively. The finally adopted value of $T(\text{Pac})$ was the average of those obtained using the different H I lines, neglecting those which are affected by atmospheric features.

Figure 1 shows the spectral regions near the Balmer and the Paschen limits. The discontinuities can be easily appreciated.

4.2. Temperature variations

Under the assumption of a constant electron temperature, RLs of heavy elements yield higher abundance values relative to hydrogen than CELs. This is a well known result that different authors have corroborated for H II regions and planetary nebulae (e.g. EPTE; Esteban et al. 2002; Liu et al. 2002, and references therein). Peimbert (1967) proposed the presence of spatial temperature fluctuations (parameterized by t^2) as the cause of this discrepancy, because CELs and RLs intensities have different dependences on the electron temperature. In addition, and for the same reason, the comparison between $T(Bac)$ or $T(Pac)$ and electron temperatures obtained from forbidden line analysis can give an indication of such fluctuations.

A complete formulation of temperature fluctuations has been developed by Peimbert (1967), Peimbert & Costero (1969) and Peimbert (1971). To derive the value of t^2 we have followed Peimbert, Peimbert, & Ruiz (2000) and Peimbert, Peimbert, & Luridiana (2002). We have assumed a 1-zone ionization scheme, and have combined the temperature derived from the ratio of the [O III] $\lambda\lambda 4363, 5007$ lines with the temperature derived from the ratio of the Paschen continuum to $I(H\beta)$, $T(Pac)$, which are given by:

$$T(O\ III) = T_0 \left[1 + \frac{1}{2} \left(\frac{91300}{T_0} - 3 \right) t^2 \right], \quad (4)$$

and

$$T(Pac) = T_0(1 - 1.67t^2); \quad (5)$$

we have labeled the resulting value as $FL - Pac$ in Table 4. Similarly we have combined $T_e(O\ III)$ with the temperature derived from the ratio of the Balmer continuum to $I(H\beta)$, $T(Bac)$, which is given by:

$$T(Bac) = T_0(1 - 1.67t^2); \quad (6)$$

we have labeled the resulting value as $FL - Bac$ in Table 4.

On the other hand, we have derived the t^2 value that produces the agreement between the ionic abundances obtained from both recombination and forbidden lines for the O^{++} ion. In particular, we have found that the RL/CEL ratio for O^{++} in this case is 1.9, which is in excellent agreement with the value found by Tsamis et al. (2003) that amounts to 1.8 (see § 6.2 for discussion about RLs abundances). Also, we have derived the t^2 value from the RL/CEL ratio of the Ne^{++} abundance, which is completely consistent with the t^2 derived from the RL/CEL ratio of O^{++} abundances. We have not considered the t^2 derived from the RL/CEL ratio of O^+ due to the high uncertainty of the abundance derived from the only suitable RL in our spectra (see § 6.2)

The values of t^2 obtained are shown in Table 4. We have adopted a final value of $t^2=0.038\pm0.009$, that is, the average of $O^{++}(R/C)$, $Ne^{++}(R/C)$, $T_e(FL - Pac)$, and $T_e(FL - Bac)$ t^2 's weighted by their uncertainties. This value is consistent with the correlation showed by Liu et al. (2000) —their Figure 8— between the ratio of CELs and RLs abundances with $T_e(FL - Bac)$. This correlation supports the idea that the disparities between electron temperatures and abundances, are closely related and probably have the same origin.

5. He⁺ abundance

There are 91 He I emission lines identified in our spectra. These lines arise mainly from pure recombination, although they may have contributions from collisional excitation and self-absorption effects. On the other hand, singlets are, in general, more suitable for deriving an accurate the He⁺/H⁺ ratio, because they are not affected by self-absorption effects. Due to the large number of singlet lines detected, and to their good signal-to-noise ratio, we have decided to derive the He⁺/H⁺ ratio making use of these lines.

To obtain He⁺/H⁺ values we need a set of effective recombination coefficients for the He and H lines, and to estimate the contribution due to collisional excitation to the helium line intensities (which is in fact rather small for singlet lines). The recombination coefficients used were those by Storey & Hummer (1995) for H I, and those by Smits (1996) and Benjamin, Skillman, & Smits (1999) for He I. The collisional contributions were estimated from the computations by Benjamin, Skillman, & Smits (1999).

In the low-density and low optical depth limit the emissivities of the helium and hydrogen lines are proportional to powers of the temperature and $T_e(\text{He II})$ is given by (Peimbert 1967):

$$\begin{aligned} T(\text{He II}) &= T_0[1 + (\langle\alpha\rangle + \beta - 1)t^2/2] \\ &= T_0(1 - 1.3t^2), \end{aligned} \tag{7}$$

where $\langle\alpha\rangle$ is the average value of the power of the temperature for the helium lines that we have used to derive the He⁺/H⁺ ratio; $\langle\alpha\rangle$ it was derived from Benjamin, Skillman, & Smits (1999) and β is the power of temperature for H β , derived from Storey & Hummer (1995). With this relation we have derived a value of $T(\text{He II})=6800\pm400$ K.

Table 5 presents the He⁺/H⁺ values obtained for the ten brightest and best observed helium singlet lines. We have obtained $He^+/H^+ = 0.087\pm0.008$ for $T(\text{He II})=6800$ K and $N_e=2800$ cm⁻³.

6. Ionic Abundances

6.1. Ionic Abundances from CELs

Ionic abundances of N^+ , O^+ , O^{++} , Ne^{++} , S^+ , S^{++} , Cl^+ , Cl^{++} , Cl^{+3} , Ar^{++} and Ar^{3+} have been determined from CELs, using the IRAF package NEBULAR (except for Cl^+ , see below). Additionally, we have determined the ionic abundances of Fe^{++} and Fe^{3+} following the methods and data discussed below. As we have shown in § 4.1, we have adopted an $N_e(\text{low})=1300 \text{ cm}^{-3}$ for the ion with the lowest ionization potential: S^+ , and the same temperature for all the ions. Ionic abundances are listed in Table 6 and correspond to the mean value of the abundances derived from all the individual lines of each ion observed (weighted by their relative strengths). The values obtained are very consistent with those derived by Tsamis et al. (2003) for the ions in common (differences not larger than 0.15 dex).

The Cl^+/H^+ ratio cannot be derived from the NEBULAR routines, instead we have used an old version of the five-level atom program of Shaw & Dufour (1995) that is described by De Robertis, Dufour, & Hunt (1987). This version uses the atomic data for Cl^+ compiled by Mendoza (1983). In any case, the atomic data for this ion and therefore the Cl^+/H^+ ratio derived are rather uncertain (Shaw 2003, personal communication).

To derive the abundances for $t^2 = 0.038$ we used the abundances for $t^2=0.00$ and the formulation of by Peimbert (1967) and Peimbert & Costero (1969) for $t^2 > 0.00$. To derive abundances for other t^2 values it is possible to interpolate or extrapolate the values presented in Table 6.

Many [Fe II] lines have been identified in the optical spectra of H II regions (Rodríguez 1996; EPTE; EPTGR). Most of these lines are severely affected by fluorescence effects (Rodríguez 1999; Verner et al. 2000). Unfortunately, we can not measure the [Fe II] λ 8617 Å line, which is almost insensitive to the effects of UV pumping. This line is precisely in one of the observational gaps of our spectroscopic configuration (see § 2). However, we do measure [Fe II] λ 7155, a line which is not much affected by fluorescence effects (Verner et al. 2000). We have derived an estimation of the Fe^+ abundance from this line assuming that $I(\lambda 7155)/I(\lambda 8616) \sim 1$ (Rodríguez 1996) and using the calculations of Bautista & Pradhan (1996). We find $\text{Fe}^+/\text{H}^+ \sim 3.5 \times 10^{-8}$, a value much lower than the values obtained for the Fe^{++} and Fe^{3+} abundances (see below). Therefore, the Fe^+ abundance will be considered negligible in what follows.

The calculations for Fe^{++} have been done with a 34 level model-atom that uses the collision strengths of Zhang (1996) and the transition probabilities of Quinet (1996). We have used 14 [Fe III] lines that do not seem to be affected by blends. We find an average

value and a standard deviation of $\text{Fe}^{++}/\text{H}^+ = (3.68 \pm 0.36) \times 10^{-7}$. Adding errors in T_e and N_e we finally obtain $12 + \log(\text{Fe}^{++}/\text{H}^+) = 5.57 \pm 0.05$.

We have detected [Fe IV] $\lambda 6739.8$, the brightest optical [Fe IV] line for the physical conditions in NGC 3576. For deriving the $\text{Fe}^{3+}/\text{H}^+$ ratio, we have used a 33-level model-atom where all collision strengths are those calculated by Zhang & Pradhan (1997), the transition probabilities are those recommended by Froese Fischer & Rubin (1998) (and those from Garstang (1958) for the transitions not considered by Froese Fischer & Rubin (1998)). Assuming an uncertainty of 50% in the intensity measured, we have derived a value of $12 + \log(\text{Fe}^{3+}/\text{H}^+) = 5.71^{+0.17}_{-0.29}$.

Values of Fe^{++} and Fe^{3+} abundances for $t^2 > 0.00$ are also shown in Table 6.

6.2. Ionic Abundances from RLs

We have measured 170 permitted lines of heavy element ions such as O I, O II, C II, Ne I, Ne II, S I, S II, N I, N II, N III, Ar I, Ar II, Si I, and Si II, most of them detected for the first time in NGC 3576.

As we noted in § 1, those permitted lines produced by recombination can give accurate determinations of ionic abundances because their relative intensities depend weakly on electron temperature and density.

Let $I(\lambda)$ be the intensity of a recombination line of an element X, i times ionized at wavelength λ ; then the abundance of the ionization state $i + 1$ of element X is given by:

$$\frac{N(\text{X}^{i+1})}{N(\text{H}^+)} = \frac{\lambda(\text{\AA})}{4861} \frac{\alpha_{eff}(\text{H}\beta)}{\alpha_{eff}(\lambda)} \frac{I(\lambda)}{I(\text{H}\beta)}, \quad (8)$$

where $\alpha_{eff}(\lambda)$ and $\alpha_{eff}(\text{H}\beta)$, are the effective recombination coefficients for the line and $\text{H}\beta$, respectively. The $\alpha_{eff}(\lambda)/\alpha_{eff}(\text{H}\beta)$ ratio is almost independent of the adopted temperatures and densities, and varies by less than a few percent within the temperature and density ranges presented in Table 3.

Following EPTE we have taken into account the abundances obtained from the intensity of each individual line and the abundances from the estimated total intensity of each multiplet, which is obtained by multiplying the sum of the intensities of the observed lines by the multiplet correction factor,

$$m_{cf} = \frac{\sum_{\text{all } i,j} s_{ij}}{\sum_{\text{obs } i,j} s_{ij}}, \quad (9)$$

where the upper sum runs over *all* the lines of the multiplet, and the lower sum runs over the *observed* lines of the multiplet. The theoretical line strengths, s_{ij} , are constructed assuming that they are proportional to the population of their parent levels assuming LTE computation predictions. The abundances derived by this manner are labeled as "Sum" in Tables 7, 8, 9, 10 and 11. This quantity corresponds to the expected abundance given by the whole multiplet. Abundances that we have taken into account are marked as boldface in Tables 7 to 11.

Ten permitted lines of C II have been measured in NGC 3576. Some of these lines (those of multiplets 6, 16.04, 17.02, 17.04 and 17.06) are $3d - 4f$ transitions and are, in principle, excited by pure recombination (see Grandi 1976). Also, the abundances obtained from them are case-independent, so we adopted the mean of the values obtained for these transitions as our final adopted C^{++}/H^+ ratio. In any case, the result for the case sensitive multiplet 3 gives a C^{++} abundance for case B consistent with that adopted. On the other hand, C II $\lambda 6578.05$ is also case sensitive and considerably affected by a telluric line. In Table 7 we summarize the abundances obtained from the different lines detected as well as the adopted average value. We used the effective recombination coefficients computed by Davey, Storey, & Kisieliu (2000). The dispersion of the abundances obtained by the different lines is very small and the final result is in very good agreement with the value obtained by Tsamis et al. (2003) from the C II $\lambda 4267$ line alone. Figure 2 shows the high signal-to-noise ratio of the four brightest C II lines detected in our spectrum.

We have detected 13 lines of N I of multiplets 1, 2 and 3. It is a well known result that starlight excitation is the main responsible of the observed strength of these lines (Grandi 1975a,b). The abundances obtained from N I lines in NGC 3576 are between 150 to 400 times higher than the abundances obtained with CELs (see Table 8), a clear indication that these lines are mainly produced by starlight excitation and not by recombination.

Abundances obtained for N^{++} are shown in Table 8. Grandi (1976) has shown that resonance fluorescence by the recombination line He I $\lambda 508.64$ is the dominant mechanism to excite the $4s^3P^0$ term of N II in the Orion Nebula, and hence it should be responsible for the strength of multiplets 3 and 5. The term $4f^3F$ cannot be reached by permitted resonance transitions and, therefore, it is excited mainly by recombination, so the abundance obtained from the $\lambda 4239.4$ line of multiplet 48 has been considered. Also, Grandi (1976) suggests that multiplets 28 and 20 could be excited by a combination of starlight and recombination. The recombination coefficients used are from Kisieliu & Storey (2002) for all multiplets except multiplet 48 for which we have adopted the recombination coefficients of Escalante & Victor (1990). Multiplets 5, 20 and 28 are strongly case-sensitive, therefore we have adopted the value given by the average of multiplets 3 and 48 in case B as a representative value of

N^{++}/H^+ .

The O^+ abundance was derived only from the O I $\lambda 7771.94$ line, because the other lines of multiplet 1 were strongly affected by telluric lines, as well as the only line of multiplet 4 detected, O I $\lambda 8446.48$. Multiplet 1 is case-independent and is produced by recombination because it corresponds to a quintuplet transition (the ground level is a triplet). The effective recombination coefficients were obtained from two sources: Péquignot, Petitjean, & Boisson (1991) and Escalante & Victor (1992). Though the results are very similar, we adopted the mean of the abundances obtained with the two different coefficients. The O^+ abundance obtained from the $\lambda 7771.94$ line is quite uncertain because it is partially blended with a sky emission line.

More than 40 lines of O II have been detected in our data. This is, along with that reported by Esteban et al. (2004) for Orion, one of the best O II recombination-line spectrum that have been observed for a Galactic H II region. O^{++}/H^+ ionic abundance ratios are presented in Table 10. Figure 3 shows the high quality of the spectrum in the zone of multiplet 1 of O II. This figure can be compared with Figure 3 of EPTE (Orion nebula), Figure 2 of Peimbert (2003) (30 Doradus) and Figure 1 of Esteban et al. (2002) (NGC 604). All these figures show the same spectral zone and a direct comparison of the quality of the spectra can be made. Effective recombination coefficients are from Storey (1994) for 3s-3p and 3p-3d transitions –LS-coupling– and from Liu et al. (1995) for 3p-3d and 3d-4f transitions –intermediate coupling–, assuming case A for doublets and case B for quartets (for definitions of cases A, B and C, see EPTE). For multiplet 15 we use the dielectronic recombination rate of Nussbaumer & Storey (1984). The intensity of the 3d-4f transitions is insensitive to optical depth effects because there are no significant radiative decays from the 4f level to the ground term (Liu et al. 1995); therefore these transitions are independent of the case assumed. In our calculations we have not considered the following lines: lines with errors higher than 40%; lines affected by blends, and the O II $\lambda 4156.54$ line of multiplet 19 because it is presumably blended with an unknown line (Liu et al. 2000). In addition to the 3d-4f transitions, the abundances determined from multiplets 1, 4, 10 and 20 are almost case independent. In contrast, multiplets 5, 19 and 25 show strong case sensitivity. This is the reason why we have adopted as representative of the O^{++}/H^+ ratio the average of values given by multiplets 1, 4, 10, 20 and 3d-4f transitions.

We have detected two 3d-4f transitions belonging to multiplet 55e of Ne II. For these transitions we have used effective recombination coefficients from recent calculations of Kissielius & Storey (unpublished), assuming LS-coupling. We have adopted the ”sum” value derived from this multiplet: $12+\log(\text{Ne}^{++}/\text{H}^+)=7.88^{+0.12}_{-0.16}$ as representative of the Ne^{++} abundance. The values derived from the individual lines as well as the average and the ”sum”

value are presented in Table 11.

7. Total Abundances

Table 12 shows the total gaseous abundances of NGC 3576 for $t^2=0.00$ and the finally adopted ones for $t^2=0.038$. To derive the total gaseous abundances, we have to assume a set of ionization correction factors, *ICF*'s, to correct for the unseen ionization stages.

The absence of He II lines in our spectra indicates that $\text{He}^{++}/\text{H}^+$ is negligible. However, the total helium abundance has to be corrected for the presence of neutral helium. Peimbert, Torres-Peimbert, & Ruiz (1992) determined an $ICF(\text{He}^0) = 1 + \text{S}^+ / (\text{S} - \text{S}^+)$, based on the similarity of the ionization potentials of He^0 (24.6 eV) and S^+ (23.3 eV). With our data, $ICF(\text{He}^0)$ amounts to 1.05 for $t^2=0.00$ and 1.04 for $t^2>0.00$. He/H is then given by:

$$\frac{N(\text{He})}{N(\text{H})} = ICF(\text{He}^0) \times \frac{N(\text{He}^+)}{N(\text{H}^+)}. \quad (10)$$

For C we only have direct determinations of C^{++} . Therefore, the C abundance is given by:

$$\frac{N(\text{C})}{N(\text{H})} = ICF(\text{C}) \times \frac{N(\text{C}^{++})}{N(\text{H}^+)}. \quad (11)$$

Taking into account the similarity between the ionization potentials of C^{++} and Ar^{++} , and the low $\text{Ar}^{3+}/\text{Ar}^{++}$ ratio obtained, the expected $\text{C}^{3+}/\text{C}^{++}$ ratio should be negligible. On the other hand, the ionization potential of C^+ (24.4 eV) is intermediate between those of S^+ (23.3 eV) and He^0 (24.6 eV); therefore we expect $\text{S}^+/\text{S} \leq \text{C}^+/\text{C} \leq \text{He}^0/\text{He}$. Moreover, to obtain the total He/H ratio we have assumed that $\text{S}^+/\text{S} = \text{He}^0/\text{He}$. Therefore, following Peimbert, Torres-Peimbert, & Ruiz (1992) we have assumed that $\text{S}^+/\text{S} = \text{C}^+/\text{C}$, so $ICF(\text{C}) = ICF(\text{He}^0)$.

To derive the total nitrogen abundance, the usual *ICF*, based on the similarity between the ionization potential of N^+ and O^+ (Peimbert & Costero 1969) is not a good approximation for ionized nebulae with high degree of ionization. Instead, following Peimbert, Torres-Peimbert, & Ruiz (1992), we have used the set of *ICF*'s obtained by Mathis & Rosa (1991). We have adopted the average of the cool and hot atmosphere results of these authors, which is 0.13 (for $t^2=0.00$) and 0.15 (for $t^2 > 0.00$) dex higher than the *ICF* determined using the standard relation, obtaining a value of $12 + \log(\text{N}/\text{H}) = 7.87$. Alternatively, we have also derived the total N abundance adding N^+/H^+ (considering $t^2=0.038$) and N^{++}/H^+ determined from permitted lines, obtaining a value of $12 + \log(\text{N}/\text{H}) = 8.07$. For comparison, we have used the value of N^{++}/H^+ calculated by Simpson et al. (1995) from FIR lines, obtaining $12 + \log(\text{N}/\text{H}) = 7.85$ for $t^2=0.038$, in excellent agreement with the N abundance derived

assuming an *ICF*. These results indicate, as Tsamis et al. (2003) have pointed out, that N II lines of multiplet 3—the dominant contributor to our adopted N^{++}/H^+ from RLs—should be slightly affected by fluorescence effects. However, assuming the faint multiplet 48 as representative of the true N^{++}/H^+ , we find $12+\log(N^{++}/H^+)=7.99\pm0.14$, which is slightly higher, but consistent within the errors, than the adopted N abundance using an *ICF*.

The absence of He II emission lines in our spectra and the similarity between the ionization potentials of He^+ and O^{++} implies the absence of O^{3+} . We have therefore assumed that:

$$\frac{N(O)}{N(H)} = \frac{N(O^+ + O^{++})}{N(H^+)}. \quad (12)$$

The only measurable CELs of Ne in the optical region are those of Ne^{++} . The ionization potential of this ion is very high (63.4 eV) and we do not expect a significant fraction of Ne^{3+} . However, Ne^+ should be important. Usually, the *ICF*(Ne^{++}) for nebulae with high ionization degree (Peimbert & Costero 1969) is given by:

$$\begin{aligned} \frac{N(Ne)}{N(H)} &= ICF(Ne) \times \left[\frac{N(Ne^{++})}{N(H^+)} \right] \\ &= \left[\frac{N(O)}{N(O^{++})} \right] \times \left[\frac{N(Ne^{++})}{N(H^+)} \right]. \end{aligned} \quad (13)$$

In the case of NGC 3576, this *ICF* gives a correction of 1.50 for $t^2=0.038$, which implies $Ne^+/Ne^{++}=0.50$ and a $12+\log(Ne/H)=8.09$. On the other hand, Simpson et al. (1995) have observed IR [Ne II] lines, obtaining $Ne^+/Ne^{++}=1.0$, but in a different zone of NGC 3576 of much lower ionization degree; adopting this value, we obtain a total Ne abundance of $12+\log(Ne/H)=8.26$, which is 0.17 dex higher than that obtained using the above equation. On the other hand, Tsamis et al. (2003) obtained $Ne^+/Ne^{++}=0.51$ for the same zone of the nebula, using the same *ICF*, so we have adopted $Ne^+/Ne^{++}=0.50$ to determine the Ne/H ratio.

We have measured CELs of two ionization stages of S, giving $S^+/S^{++}=0.04$. An ionization correction factor, *ICF*(S), to take into account the presence of S^{3+} , has to be considered. We have adopted the following relation from Stasińska (1978):

$$ICF(S) = \left[1 - \left(1 - \frac{N(O^+)}{N(O)} \right)^3 \right]^{-1/3}, \quad (14)$$

and

$$\frac{N(S)}{N(H)} = ICF(S) \times \frac{N(S^+ + S^{++})}{N(H^+)}, \quad (15)$$

which is based in photoionization models of H II regions; using this relation we derived a value of $ICF(S)=1.1$. On the other hand, based in the correlation between N^{++}/N^+ *vs.* S^{3+}/S^{++} from ISO observations of compact H II regions obtained by Martín-Hernández et al. (2002) we estimate an $ICF(S)=1.2$, which is in good agreement with that obtained from the above equation.

We have measured lines of all possible ionization stages of chlorine: Cl^+ , Cl^{++} and Cl^{3+} . We have derived the Cl/H ratio adding the three ionic abundance determinations available for this element. However, as we discussed in § 6.1, Cl^+ atomic data are probably not reliable. So, alternatively, to take into account the Cl^+ fraction, we have adopted the relation by Peimbert & Torres-Peimbert (1977): $ICF(Cl)=1/(1-S^+/S)$. With our data an $ICF(Cl)=1.04$ is derived. With this ICF , for $t^2>0.00$, Cl abundance is 0.02 dex lower than taking into account the Cl^+/H^+ ratio, showing that Cl^+ is in fact only a small fraction of the total amount of Cl.

For argon we have determinations of Ar^{++} and Ar^{3+} . We obtain $Ar^{3+}/Ar^{++}=0.007$, indicating that most Ar is in the form of Ar^{++} . However, some contribution of Ar^+ is expected. Martín-Hernández et al. (2002) have obtained a correlation between N^{++}/N^+ *vs.* Ar^{++}/Ar^+ from ISO observations of compact H II regions; using that result we estimate an $ICF(Ar)=1.1$.

Finally, we have measured lines of the three main stages of ionization of iron: Fe^+ , Fe^{++} and Fe^{3+} . Rodríguez (1999) has shown evidences for the existence of fluorescence excitation in the formation process of the observed [Fe II] lines, so the determination of the Fe^+/H^+ ratio is not reliable. On the other hand we have obtained the Fe^{3+}/H^+ ratio from the [Fe IV] $\lambda 6739.8$ line which has an uncertainty of about 50%. In Table 12, two values are given for the Fe abundance. The first one has been derived from [Fe III] and the ICF of Rodríguez & Rubin (2004) to take into account the fractions of Fe^+ and, mainly, Fe^{3+} in the nebula:

$$\frac{N(Fe)}{N(H)} = \left[\frac{N(O^+)}{N(O^{++})} \right]^{0.09} \times \frac{N(Fe^{++})}{N(O^+)} \times \frac{N(O)}{N(H)}. \quad (16)$$

The second value for the Fe abundance is just the sum of the derived ionic abundances, taking into account only Fe^{++} and Fe^{3+} –the contribution of Fe^+ should be very small (see § 6.1). For the handful of objects where [Fe IV] emission has been previously measured (see Rodríguez 2003, and references therein) the Fe abundances based on the sum of the ionic abundances are systematically lower, by factors 2–4, than the the total abundances implied by Fe^{++} and the above ICF . In our case, there are no differences in the abundances derived from both methods for $t^2=0.00$, and for $t^2>0.00$ the sum of the ionic abundances is only a factor of 1.3 lower than the $Fe^{++}+ICF$ abundance. This fact could be due either to the lower degree of ionization shown by NGC 3576 respect to the other objects (see Rodríguez 2003;

Rodríguez & Rubin 2004) or to our possible overestimation of the intensity of the extremely weak [Fe IV] $\lambda 6739.8$ line.

8. Discussion

In Table 13 we compare the gaseous abundances of NGC 3576 with those derived by Simpson et al. (1995) (FIR), Girardi et al. (1997) (optical CELs) and Tsamis et al. (2003) (optical RLs and CELs). It can be seen that our values are in very good agreement with those in common with Tsamis et al. (2003) and rather similar to the values found by Simpson et al. (1995). In contrast, the abundances differ to the values obtained by Girardi et al. (1997), probably because their slit positions are quite far from ours. The main differences between our results and those of Tsamis et al. (2003) are in the total abundances. The different set of *ICF* scheme used, could explain those differences.

To compare the NGC 3576 abundances with those of the Sun, it is necessary to estimate the fraction of heavy elements embedded in dust grains. We have assumed that the fraction of heavy elements trapped in dust is the same for NGC 3576 and Orion; therefore, following EPTE we have added 0.10 dex, 0.08 dex, and 1.37 dex to the gaseous C, O and Fe abundances, respectively. For N, S, and Cl, no dust correction was applied since they are not significantly depleted in the neutral ISM (Savage & Sembach 1996). For He, Ne, and Ar, no correction was applied since they are noble gases.

For the Sun: He comes from Christensen-Dalsgaard (1998), C and N from Asplund (2003), O, Ne, and Ar from Asplund et al. (2004), and S, Cl, and Fe from Grevesse & Sauval (1998).

In Table 14 we compare NGC 3576 gas+dust abundances with the solar values. We expect a higher O/H value of about 0.15 dex in NGC 3576 than in the Sun in excellent agreement with the observed value. Our estimate is based on the following considerations: *i*) from the chemical evolution models for the Galaxy (Carigi 2003; Akerman et al. 2004) it is found that the O/H ratio in the interstellar medium at the solar galactocentric distance has increased by 0.12 dex since the Sun was formed, *ii*) there is a galactocentric difference of 0.6 kpc in the distance between the Sun and NGC 3576, and *iii*) the O/H gradient amounts to $-0.061 \text{ dex kpc}^{-1}$ (see below). Based on the same considerations a very good agreement is also found for the excesses obtained for Ne and S, the relatively large difference in the Ar/H value is probably due in part to the uncertain *ICF* we have used.

The results of this work, along with those of EPTE, EPTGR and Esteban et al. (1999b) for Orion, M8 and M17 make possible to present an approach to gas phase abundance

gradients in our Galaxy based exclusively on recombination lines. Figure 4 shows the C/H and O/H abundances derived for these objects. The galactocentric distances have been obtained from the complete survey of Russeil (2003) of star-forming complexes in our galaxy, using stellar distances to derive their galactocentric radius, and adopting a solar galactocentric radius of 8.0 kpc. We found a gradient of $-0.061 \text{ dex kpc}^{-1}$ for O/H, which is somewhat higher than the values obtained by Esteban et al. (1999b) and Deharveng et al. (2000), which are -0.049 and $-0.040 \text{ dex kpc}^{-1}$ respectively, and also somewhat higher than the value found for M101 from O RLs by Esteban et al. (2002), which is $-0.038 \text{ dex kpc}^{-1}$. On the other hand, the gradient we derive for C/H is $-0.090 \text{ dex kpc}^{-1}$, which is very similar to the Galactic one derived by Esteban et al. (1999b) and revised by Esteban et al. (2002) of $-0.086 \text{ dex kpc}^{-1}$. Our value of the C gradient is consistent with that obtained by Rolleston et al. (2000) for B stars: -0.07 ± 0.02 , assuming LTE model atmospheres and LTE line formation. However, the absolute C abundances obtained for nearby B stars are systematically much lower than the values obtained for the Sun and G-F stars and H II regions of the solar neighborhood. This could be due to NLTE effects or problems with the C atomic model used (Herrero 2003).

Also in Figure 4 we show the solar O/H and C/H values and the values expected for the interstellar medium at the solar galactocentric distance taking into account the chemical evolution of the Galaxy. From the models by Carigi (Carigi 2003; Akerman et al. 2004) it is found that the increase in O/H and C/H of the interstellar medium since the Sun was formed amounts to 0.12 dex and 0.24 dex respectively.

The C/O gradient is an important constraint for chemical evolution models and the star formation history across the Galactic disk. The bulk of these two elements are, in principle, produced by stellar progenitors of different initial mass ranges. We derive a C/O gradient of $-0.029 \text{ dex kpc}^{-1}$, which is similar to that given previously by Esteban et al. (2002): $-0.037 \text{ dex kpc}^{-1}$; and not too different to that obtained by Smartt et al. (2001) for B stars: $-0.05 \text{ dex kpc}^{-1}$. Garnett et al. (1999) have obtained similar C/O gradients in two external spiral galaxies from C abundances derived from UV semi-forbidden lines.

9. SUMMARY

We present echelle spectroscopy in the 3100-10400 Å range for the H II region NGC 3576 (Gum38a). We have measured the intensities of 461 emission lines; 170 of them are permitted lines of heavy elements. This is the most complete list of emission lines obtained for this object and one of the largest collections ever taken for a Galactic H II region.

We have derived physical conditions of the nebula making use of many different line intensities and continuum ratios. The chemical abundances have been derived for a large number of ions and different elements. We find excellent agreement between the C^{++}/H^+ ratio obtained from the brightest C II RL, $\lambda 4267 \text{ \AA}$ and others corresponding to 3d-4f transitions of this ion. All these transitions are—in principle—excited by pure recombination and give a precise determination of the C^{++} abundance. We find also a good agreement between the O^{++}/H^+ ratios derived from RLs of multiplets 1, 4, 10, 20 and 3d-4f, which are case-independent transitions and produced largely by recombination. Alternatively, abundances derived for N^{++} for different multiplets show differences as high as a factor of 3. These differences probably are due to fluorescence effects. Finally, we have also determined abundances of O^+ and Ne^{++} from RLs for the first time in this object.

We have obtained an average $t^2=0.038\pm0.009$ both by comparing the O^{++} and Ne^{++} ionic abundances derived from CELs to those derived from RLs, and by comparing the electron temperatures determined from ratios of CELs to those obtained from the Balmer and Paschen continua. It is remarkable that the four individual values obtained are almost coincident. The adopted average value of t^2 has been used to correct the ionic abundances determined from CELs.

We have estimated the C/H, O/H, and C/O Galactic radial abundance gradients making only use of determinations based on RLs of H II regions, obtaining values of -0.090, -0.061, and -0.029, respectively. These estimation is based in four objects covering a rather narrow interval of galactocentric distances (from 6 to 9 kpc).

We would like to thank R. Kisielius and P. J. Storey for providing us with their latest calculations of effective recombination coefficients for Ne, D.P. Smits for providing us unpublished atomic calculations for He, and L. Carigi for testing our results with her chemical evolution models. We would also like to thank an anonymous referee for his/her valuable comments. This work has been partially funded by the Spanish Ministerio de Ciencia y Tecnología (MCyT) under project AYA2001-0436. MP received partial support from DGAPA UNAM (grant IN 114601). MTR received partial support from FONDAP(15010003), a Guggenheim Fellowship and Fondecyt(1010404). MR acknowledges support from Mexican CONACYT project J37680-E.

REFERENCES

- Akerman, C. J., Carigi, L., Nissen, P. E., Pettini, M., & Asplund, M. 2004, *A&A*, 414, 931
- Asplund, M. 2003, in: *ASP Conference Series 304, CNO in the Universe*, ed. C. Charbonnel,

- D, Schaerer, & G. Meynet, 275
- Asplund, M., Grevesse, N., Sauval, A. J, Allende-Prieto, C., & Kiselman, D. 2004, A&A, in press, (astro-ph/0312290)
- Baldwin, J.A., Verner, E.M., Verner, D.A., Ferland, G.J., Martin, P.G., Korista, K.T., & Rubin, R.H. 2000, ApJS, 129, 229
- Bautista, M.A., & Pradhan, A.K. 1996, A&AS, 115, 551
- Benjamin, R.A., Skillman, E.D., & Smits, D.P. 1999, ApJ, 514, 307
- Boreiko, R.T., & Betz, A.L. 1997, ApJS, 111, 409
- Brown, R.L., & Mathews, W.G. 1970, ApJ, 160, 939
- Christensen-Dalsgaard, J. 1998, Space Sci. Rev., 85, 19
- Carigi, L. 2003, MNRAS, 339, 825
- Davey, A.R., Storey, P.J., & Kisieliuss, R. 2000, A&A, 142, 85
- Deharveng, L., Peña, M., Caplan, J., & Costero, R. 2000, MNRAS, 311, 329
- De Robertis, M.M., Dufour, R.J., & Hunt, R.W. 1987, JRASC, 81, 195
- D’Odorico, S., Cristiani, S., Dekker, H., Hill, V., Kaufer, A., Kim, T., & Primas, F. 2000, Proc. SPIE, 4005, 121
- Escalante, V., & Victor, G.A. 1990, ApJS, 73, 513
- Escalante, V., & Victor, G.A. 1992, Planet. Space Sci., 40, 1705
- Esteban, C. 2002, Rev. Mexicana. Astron. Astrofís. Ser. Conf., 12, 56
- Esteban, C., Peimbert, M., García-Rojas, J., Peimbert, A., Ruiz, M.T., & Rodríguez, M. 2004, in preparation
- Esteban, C., Peimbert, M., Torres-Peimbert, S., & Escalante, V. 1998, MNRAS, 295, 401 (EPTE)
- Esteban, C., Peimbert, M., Torres-Peimbert, S., & García-Rojas, J. 1999b, Rev. Mexicana. Astron. Astrofís., 35, 65
- Esteban, C., Peimbert, M., Torres-Peimbert, S., García-Rojas, J., & Rodríguez, M. 1999a, ApJS, 120, 113 (EPTGR)

- Esteban, C., Peimbert, M., Torres-Peimbert, S., & Rodríguez, M. 2002, *ApJ*, 581, 241
- Feklistova, T., Golovatyj, V.V., Kholtygin, A.F., & Sapar, A. 1994, *Baltic Astronomy*, 3, 292
- Figuêredo, E., Blum, R.D., Damineli, A., & Conti, P.S. 2002, *AJ*, 124, 2739
- Froese Fischer C., Rubin R. H., 1998, *J. Phys. B: At. Mol. Opt. Phys.*, 31, 1657
- Garnett, D. R., Shields, G. A., Peimbert, M., Torres-Peimbert, S., Skillman, E. D., Dufour, R. J., Terlevich, E., & Terlevich, R. J., 1999, *ApJ*, 513, 168
- Garstang R. H., 1958, *MNRAS*, 118, 572
- Girardi, L., Bica, E., Pastoriza, M.G., & Winge, C. 1997, *ApJ*, 486, 847
- Grandi, S.A. 1975a, *ApJ*, 166, 465
- Grandi, S.A. 1975b, *ApJ*, 199, L43
- Grandi, S.A. 1976, *ApJ*, 206, 658
- Grevesse, N., & Sauval, A. J. 1998, *Space Sci. Rev.*, 85, 161
- Herrero, A., 2003, in: *ASP Conference Series 304, CNO in the Universe*, ed. C. Charbonnel, D, Schaerer, & G. Meynet, 10
- Howard, I.D., & Murray, J. 1990, *SERC Starlink User Note No. 50*
- Humphreys, R.M. 1978, *ApJS*, 38, 309
- Kisielius, R., & Storey, P. J. 2002, *A&A*, 387, 1135
- Liu, X.-W. 2002, *Rev. Mexicana. Astron. Astrofís. Ser. Conf.*, 12, 70
- Liu, X.-W. 2003, in *IAU Symposium 209, Planetary Nebulae and Their Role in the Universe*, ed. S. Kwok, M. Dopita, & R. Sutherland (San Francisco: ASP), 339
- Liu, X.-W., Luo, S.-G., Barlow, M.J., Danziger, I.J., & Storey, P.J. 2001, *MNRAS*, 327, 141
- Liu, X.-W., Storey, P.J., Barlow, M.J., & Clegg, R.E.S. 1995, *MNRAS*, 272, 369
- Liu, X.-W., Storey, P.J., Barlow, M.J., Danziger, I.J., Cohen, M., & Bryce, M. 2000, *MNRAS*, 312, 585
- Martín-Hernández, N.L., Peeters, E., Morisset, C., et al. 2002, *A&A*, 381, 606

- Mathis, J.S., & Rosa, M.R. 1991, *A&A*, 245, 625
- Mendoza C., 1983, Flower D. R., Reidel D., eds, *Proc. IAU Symp. 103, Planetary Nebulae*, Kluwer, Dordrecht, 143
- Moore, C.E. 1945, *A Multiplet Table of Astrophysical Interest (Contributions from the Princeton University Observatory, No. 20. Princeton: The Observatory)*
- Moore, C.E. 1993, *Tables of Spectra of Hydrogen, Carbon, Nitrogen and Oxygen Atoms and Ions* (Boca Raton: CRC)
- Nussbaumer, H., & Storey, P.J. 1984, *A&AS*, 56, 293
- O'Dell, C.R., Peimbert, M., & Peimbert, A. 2003, *AJ*, 125, 2590
- Osterbrock, D.E., Tran, H.D., & Veilleux, S. 1992, *ApJ*, 389, 305
- Peimbert, A. 2003, *ApJ*, 584, 735
- Peimbert, A., Peimbert, M., & Luridiana, V. 2002, *ApJ*, 565, 668
- Peimbert, M. 1967, *ApJ*, 150, 825
- Peimbert, M. 1971, *Bol. Obs. Tonantzintla y Tacubaya*, 6, 29
- Peimbert, M., & Costero, R. 1969, *Bol. Obs. Tonantzintla y Tacubaya*, 5, 3
- Peimbert, M., Peimbert, A., & Ruiz, M.T. 2000, *ApJ*, 541, 688
- Peimbert, M., Peimbert, A., Ruiz, M.T., & Esteban, C. 2004, *ApJS*, 150, 431
- Peimbert, M., Storey, P.J., & Torres-Peimbert, S. 1993, *ApJ*, 414, 626
- Peimbert, M., & Torres-Peimbert, S. 1977, *MNRAS*, 179, 217
- Peimbert, M., Torres-Peimbert, S., & Ruiz, M.T. 1992, *Rev. Mexicana. Astron. Astrofís.*, 24, 155
- Péquignot, D., & Baluteau, J.-P. 1988, *A&A*, 206, 298
- Péquignot, D., Petitjean, P., & Boisson, C. 1991, *A&A*, 251, 680
- Quinet P., 1996, *A&AS*, 116, 573
- Rodgers, A.W., Campbell, C.T., & Whiteoak, J.B. 1960, *MNRAS*, 121, 103

- Rodríguez, M. 1996, *A&A*, 313, L5
- Rodríguez, M. 1999, *A&A*, 348, 222
- Rodríguez, M. 2002, *A&A*, 389, 556
- Rodríguez, M. 2003, *ApJ*, 590, 296
- Rodríguez, M., & Rubin, R.H. 2004, in *Recycling Intergalactic and Interstellar Matter*, IAU Symposium No 217, in press (astro-ph/0312246)
- Rolleston, W.R.J., Smartt, S.J., Dufton, P.L., & Ryans, R.S.I. 2000, *A&A*, 363, 537
- Rubin, R.H., Martin, P.G., Dufour, R.J., Ferland, G.J., Blagrove, K.P.M., Liu, X.-W., Nguyen, J.F., & Baldwin, J.A. 2003, *MNRAS*, 340, 362
- Ruiz, M.T., Peimbert, A., Peimbert, M., & Esteban, C. 2003, *ApJ*, 595, 247
- Russeil, D. 2003, *A&A*, 397, 133
- Savage, B.D., & Mathis, J.S. 1979, *ARA&A*, 17, 73
- Savage, B.D., & Sembach, K.R. 1996, *ApJ*, 457, 211
- Sharpee, B., Williams, R., Baldwin, J.A., & van Hoof, P.A.M. 2003, *ApJS*, 149, 157
- Shaw, R.A., & Dufour, R. 1995, *PASP*, 107, 896
- Smartt, S.J., Venn, K.A., Dufton, P.L., Lennon, D.J., Rolleston, W.R.J., & Keenan, F.P. 2001, *A&A*, 367, 86
- Smits, D.P. 1996, *MNRAS*, 278, 683
- Simpson, J.P., Colgan, S.W.J., Rubin, R.H., Erickson, E.F., & Haas, M.R. 1995, *ApJ*, 444, 721
- Storey, P. J. 1994, *A&A*, 282, 999
- Storey, P. J., & Hummer, D. G. 1995, *MNRAS*, 272, 41
- Stasińska, G. 1978, *A&A*, 66, 257
- Torres-Peimbert, S., & Peimbert, M. 2003, in *IAU Symposium 209, Planetary Nebulae and Their Role in the Universe*, ed. S. Kwok, M. Dopita, & R. Sutherland (San Francisco: ASP), 363

- Tsamis, Y.G., Barlow, M.J., Liu, X.-W., Danziger, I.J., & Storey, P.J. 2003, MNRAS, 338, 687
- Verner, E.M., Verner, D.A., Baldwin, J.A., Ferland, G.J., & Martin, P.G. 2000, ApJ, 543, 831
- Wiese, W.L., Smith, M.W., & Glennon, B.M. 1966, Atomic Transition Probabilities. (NBS 4)(Washington: NBS)
- Wiese, W.L., Fuhr, J.R., & Deters, T.M. 1996, in Atomic Transition Probabilities of Carbon, Nitrogen, and Oxygen: A Critical Data Compilation, Journal of Physical and Chemical Data, Monograph No. 7
- Zhang H. L., 1996, A&AS, 119, 523
- Zhang H. L., & Pradhan A. K., 1997, A&AS, 126, 373

Table 1. Log of observations.

Object	$\Delta\lambda$ (\AA)	Exp. Time (s)
NGC 3576	B1: 3000–3900	60, 3×600
"	B2: 3800–5000	120, 3×1800
"	R1: 4700–6400	60, 3×600
"	R2: 6300–10400	120, 3×1800

Table 2. Observed and reddening corrected line ratios ($F(H\beta) = 100$) and line identifications.

λ_0 (Å)	Ion	Mult.	λ (Å)	$F(\lambda)^a$	$I(\lambda)^b$	Err(%)	notes
3187.84	He I	3	3187.57	0.865	2.837	7	
3354.55	He I	8	3354.31	0.076	0.222	17	
3447.59	He I	7	3447.40	0.131	0.311	12	
3478.97	He I	48	3478.79	0.035	0.083	27	
	?		3485.20	0.047	0.110	22	
3487.73	He I	42	3487.54	0.047	0.110	22	
3498.66	He I	40	3498.41	0.075	0.173	16	
3512.52	He I	38	3512.35	0.069	0.160	17	
3530.50	He I	36	3530.28	0.099	0.228	14	
3554.42	He I	34	3554.17	0.133	0.300	12	
3587.28	He I	32	3587.05	0.146	0.325	11	
3613.64	He I	6	3613.42	0.212	0.467	9	
3634.25	He I	28	3634.05	0.233	0.507	8	
3657.27	H I	H36	3657.02	0.034	0.073	27	
3657.92	H I	H35	3657.67	0.030	0.065	30	
3658.64	H I	H34	3658.42	0.031	0.066	30	
3659.42	H I	H33	3659.19	0.051	0.109	21	
3660.28	H I	H32	3660.05	0.077	0.166	16	
3661.22	H I	H31	3661.02	0.097	0.209	14	
3662.26	H I	H30	3661.98	0.092	0.199	14	
3663.40	H I	H29	3663.18	0.123	0.263	12	
3664.68	H I	H28	3664.48	0.138	0.296	11	
3666.10	H I	H27	3665.89	0.153	0.327	10	
3667.68	H I	H26	3667.45	0.177	0.379	10	
3669.47	H I	H25	3669.25	0.193	0.413	9	
3671.48	H I	H24	3671.27	0.221	0.473	8	
3673.76	H I	H23	3673.56	0.259	0.552	8	
3676.37	H I	H22	3676.15	0.279	0.593	8	
3679.36	H I	H21	3679.14	0.320	0.670	7	
3682.81	H I	H20	3682.58	0.352	0.747	7	
3686.83	H I	H19	3686.62	0.413	0.875	6	
3691.56	H I	H18	3691.34	0.478	1.009	6	
3697.15	H I	H17	3696.93	0.577	1.215	5	
3703.86	H I	H16	3703.64	0.647	1.357	5	
3705.04	He I	25	3704.79	0.346	0.726	7	
3711.97	H I	H15	3711.76	0.763	1.593	5	
3721.83	[S III]	2F	3721.62	1.588	3.301	4	}
3721.94	H I	H14					
3726.03	[O II]	1F	3725.85	37.793	78.353	4	
3728.82	[O II]	1F	3728.59	26.222	54.282	4	
3734.37	H I	H13	3734.15	1.259	2.599	4	
3750.15	H I	H12	3749.93	1.550	3.171	4	
3770.63	H I	H11	3770.41	1.931	3.905	4	
3784.89	He I	64	3784.69	0.028	0.057	14	
3797.90	H I	H10	3797.68	2.763	5.528	4	
3805.78	He I	63	3805.51	0.027	0.053	15	
3819.61	He I	22	3819.40	0.596	1.171	4	

Table 2—Continued

λ_0 (Å)	Ion	Mult.	λ (Å)	$F(\lambda)^a$	$I(\lambda)^b$	Err(%)	notes
3833.57	He I	62	3833.28	0.039	0.076	11	
3835.39	H I	H9	3835.16	3.840	7.487	3	
3838.37	N II	30	3837.95	0.048	0.093	10	
3856.02	Si II	1	3855.79	0.112	0.216	6	
3856.13	O II	12					
3862.59	Si II	1	3862.37	0.099	0.191	7	
3867.48	He I	20	3867.29	0.086	0.164	7	
3868.75	[Ne III]	1F	3868.51	11.373	21.748	3	
3871.82	He I	60	3871.56	0.079	0.150	7	
3888.65	He I	2	3888.72	8.475	16.015	3	
3889.05	H I	H8					
	?		3914.32	0.007	0.014	36	
3916.38	N II		3916.17	0.007	0.014	35	
3918.98	C II	4	3918.72	0.030	0.055	14	
3920.68	C II	4	3920.43	0.054	0.100	9	
3926.53	He I	58	3926.33	0.065	0.120	8	
3964.73	He I	5	3964.50	0.523	0.944	3	
3967.46	[Ne III]	1F	3967.23	3.456	6.229	3	
3970.07	H I	H7	3969.84	8.732	15.713	3	
3998.76	S II	59	3998.53	0.009	0.016	31	
4008.36	[Fe III]	4F	4008.05	0.029	0.049	14	f
4009.22	He I	55	4009.01	0.093	0.159	7	
4023.98	He I	54	4023.58	0.013	0.023	23	
4026.08	N II	40	4025.97	1.241	2.112	3	
4026.21	He I	18					
4032.81	S II	59	4032.49	0.010	0.016	29	
4068.60	[S II]	1F	4068.39	0.685	1.140	3	
4069.62	O II	10	4069.53	0.084	0.139	7	
4069.89	O II	10					
4072.15	O II	10	4071.93	0.051	0.085	9	
4075.86	O II	10	4075.62	0.065	0.108	8	
4076.35	[S II]	1F	4076.14	0.232	0.385	4	
4083.90	O II	48b	4083.52	0.011	0.017	28	
4085.11	O II	10	4084.90	0.015	0.024	22	
4087.15	O II	48c	4086.88	0.016	0.026	21	
4089.29	O II	48a	4089.02	0.027	0.044	14	e
4097.25	O II	20	4097.04	0.032	0.052	13	
4097.26	O II	48b					
4101.74	H I	H6	4101.50	15.369	24.681	3	
4110.78	O II	20	4110.51	0.009	0.015	30	
4119.22	O II	20	4119.05	0.014	0.023	22	
4120.84	He I	16	4120.58	0.143	0.232	5	e
4129.32	O II	19	4129.00	0.006	0.009	:	
4131.72	Ar II		4131.48	0.008	0.013	33	g
4132.80	O II	19	4132.57	0.022	0.035	17	
4143.76	He I	53	4143.52	0.178	0.284	4	
4145.91	O II	106	4145.64	0.012	0.019	26	
4146.09	O II	106					
4153.30	O II	19	4153.05	0.027	0.043	14	
4156.54	O II	19	4156.03	0.018	0.028	19	f
4168.97	He I	52	4168.76	0.041	0.064	11	
4169.22	O II	19					
4185.45	O II	36	4185.22	0.022	0.034	17	

Table 2—Continued

λ_0 (Å)	Ion	Mult.	λ (Å)	$F(\lambda)^a$	$I(\lambda)^b$	Err(%)	notes
4189.79	O II	36	4189.49	0.017	0.026	20	
4201.35	N II	49	4201.01	0.009	0.014	30	g
4236.91	N II	48	4236.64	0.007	0.011	36	
4241.78	N II	48	4241.53	0.009	0.014	31	
4242.50	N II	48	4242.29	0.006	0.010	39	
4243.97	[Fe II]	21F	4243.76	0.019	0.028	18	
4267.15	C II	6	4266.91	0.199	0.295	4	
4275.55	O II	67a	4275.33	0.013	0.019	24	e
4276.75	O II	67b	4276.51	0.038	0.055	11	e
4276.83	[Fe II]	21F					
4285.69	O II	78b	4285.28	0.010	0.015	29	
4287.39	[Fe II]	7F	4287.19	0.055	0.081	9	
4303.61	O II	65a	4303.56	0.021	0.031	17	
4303.82	O II	53a					
4317.14	O II	2	4316.86	0.018	0.026	19	
4319.63	O II	2	4319.35	0.014	0.019	23	
4326.40	O I		4326.14	0.019	0.027	18	
4332.71	O II	65b	4332.45	0.009	0.013	:	
4336.79	[Cr II]		4336.53	0.040	0.056	11	
4340.47	H I	H5	4340.20	32.386	45.921	2	
4345.55	O II	65c	4345.22	0.040	0.057	11	
4345.56	O II	2					
4349.43	O II	2	4349.18	0.047	0.067	10	
4359.33	[Fe II]	7F	4359.13	0.037	0.051	12	
4363.21	[O III]	2F	4362.95	0.915	1.279	2	
4366.89	O II	2	4366.62	0.029	0.040	14	
4368.25	O I	5	4368.10	0.050	0.069	9	
4372.43	[Fe II]	21F	4372.24	0.006	0.009	:	
4387.93	He I	51	4387.67	0.404	0.555	3	
4391.99	Ne II	55e	4391.66	0.013	0.018	:	
4409.30	Ne II	55e	4408.89	0.014	0.024	:	
4413.78	[Fe II]	7F	4413.57	0.029	0.050	14	
4414.90	O II	5	4414.64	0.017	0.029	20	
4416.27	[Fe II]	6F	4416.07	0.039	0.067	11	
4416.97	O II	5	4416.71	0.018	0.031	19	
4437.55	He I	50	4437.29	0.048	0.080	10	
4452.10	[Fe II]	7F	4451.91	0.021	0.035	17	
4452.37	O II	5					
4471.09	He I	14	4471.24	3.435	5.503	2	
4474.90	[Fe II]	7F	4474.72	0.015	0.024	22	
4491.07	C II	86a	4491.03	0.014	0.022	22	
4491.23	O II						
4562.60	Mg I]	1	4562.17	0.0095	0.0135	30	
4571.10	Mg I]	1	4570.87	0.014	0.019	23	
4590.97	O II	15	4590.67	0.021	0.029	17	
4595.95	O II	15	4595.92	0.018	0.025	19	
4596.18	O II	15					
4601.48	N II	5	4601.25	0.010	0.013	29	
4602.13	O II	92b	4601.72	0.004	0.006	:	
4607.06	[Fe III]	3F	4606.85	0.035	0.047	12	
4607.16	N II	5					
4609.44	O II	92a	4609.16	0.018	0.024	19	
4613.68	O II	92b	4613.58	0.008	0.010	35	
4613.87	N II	5					

Table 2—Continued

λ_0 (Å)	Ion	Mult.	λ (Å)	$F(\lambda)^a$	$I(\lambda)^b$	Err(%)	notes
4621.39	N II	5	4621.12	0.017	0.023	20	
4624.11	S II		4623.85	0.005	0.006	:	g
4630.54	N II	5	4630.26	0.043	0.055	10	
4634.14	N III	2	4633.82	0.012	0.015	26	
4638.86	O II	1	4638.57	0.057	0.074	8	
4640.64	N III	2	4640.38	0.027	0.034	14	
4641.81	O II	1	4641.53	0.103	0.132	6	
4643.06	N II	5	4642.78	0.021	0.027	17	
4649.13	O II	1	4648.86	0.114	0.145	5	
4650.84	O II	1	4650.54	0.055	0.069	9	
4658.10	[Fe III]	3F	4657.87	0.438	0.552	2	
4661.63	O II	1	4661.30	0.072	0.090	7	e
4667.01	[Fe III]	3F	4666.70	0.024	0.030	16	f
4673.73	O II	1	4673.39	0.011	0.013	27	
4676.24	O II	1	4675.92	0.032	0.040	13	
4696.36	O II	1	4696.04	0.006	0.007	:	
4699.21	O II	25	4698.80	0.006	0.007	:	
4705.35	O II	25	4705.09	0.007	0.008	38	
4701.53	[Fe III]	3F	4701.33	0.121	0.144	5	
4711.37	[Ar IV]	1F	4711.12	0.042	0.050	10	
4713.14	He I	12	4712.90	0.525	0.620	2	
4733.91	[Fe III]	3F	4733.65	0.048	0.055	10	
4740.16	[Ar IV]	1F	4739.95	0.045	0.051	10	
4752.96	O II	94	4752.60	0.007	0.008	35	
4754.69	[Fe III]	3F	4754.50	0.082	0.092	7	
4769.43	[Fe III]	3F	4769.23	0.048	0.053	10	
4777.68	[Fe III]	3F	4777.47	0.024	0.027	15	
4779.71	N II	20	4779.34	0.008	0.009	32	
4788.13	N II	20	4787.73	0.016	0.017	20	
4792.01	S II	46	4791.76	0.008	0.009	33	
4802.23	C II		4802.16	0.009	0.010	30	
4803.29	N II	20	4802.99	0.018	0.019	19	
4814.55	[Fe II]	20F	4814.31	0.031	0.033	21	
4815.51	S II	9	4815.26	0.016	0.017	21	
4861.33	H I	H4	4861.09	100.000	100.000	0.7	
4881.00	[Fe III]	2F	4880.83	0.214	0.209	5	
4889.63	[Fe II]	4F	4889.44	0.014	0.014	23	}
4889.70	[Fe II]	3F					
4902.65	Si II	7.23	4902.41	0.014	0.014	22	
4905.34	[Fe II]	20F	4905.17	0.015	0.015	21	
4921.93	He I	48	4921.69	1.258	1.183	2	
4924.50	[Fe III]	2F	4924.32	0.045	0.042	10	}
4924.50	O II	28					
4930.50	[Fe III]	1F	4930.32	0.011	0.010	27	
4931.32	[O III]	1F	4930.97	0.054	0.051	19	
4958.91	[O III]	1F	4958.69	134.179	121.335	0.7	
4985.90	[Fe III]	2F	4985.58	0.041	0.036	11	
4987.20	[Fe III]	2F	4987.00	0.033	0.029	12	

Table 2—Continued

λ_0 (Å)	Ion	Mult.	λ (Å)	$F(\lambda)^a$	$I(\lambda)^b$	Err(%)	notes
4994.37	N II	94	4994.16	0.033	0.029	28	
4996.98	O II		4996.76	0.043	0.037	23	g
5001.47	N II	19	5001.15	0.042	0.037	24	
5006.84	[O III]	1F	5006.66	408.677	353.023	0.7	
5011.30	[Fe III]	1F	5011.16	0.060	0.051	19	
5015.68	He I	4	5015.47	2.645	2.266	2	
5035.79	[Fe II]	4F	5035.59	0.025	0.021	34	
5041.03	Si II	5	5040.82	0.255	0.213	7	
5041.98	O II	23.01	5041.78	0.012	0.010	:	
5045.10	N II	4	5044.79	0.029	0.024	30	
5047.74	He I	47	5047.61	0.389	0.323	5	e
5055.98	Si II	5 }	5055.84	0.262	0.216	7	
5056.31	Si II	5 }					
5084.77	[Fe III]	1F	5084.58	0.012	0.010	:	
5111.63	[Fe II]	19F	5111.51	0.016	0.012	:	
5121.83	C II		5121.61	0.011	0.009	:	
5146.70	[Fe III]		5146.49	0.014	0.011	:	g
5158.78	[Fe II]	19F	5158.62	0.063	0.047	18	
5191.82	[Ar III]	3F	5191.50	0.099	0.072	13	
5197.90	[N I]	1F	—	—	—	—	c
5200.26	[N I]	1F	—	—	—	—	c
5261.61	[Fe II]	19F	5261.51	0.053	0.037	20	
5270.40	[Fe III]	1F	5270.33	0.332	0.227	6	
5273.35	[Fe II]	18F	5273.19	0.025	0.017	34	
5275.12	O I	27	5275.17	0.022	0.015	37	
5276.85	C II	56	5276.55	0.015	0.010	:	g
5299.00	O I	26	5298.99	0.040	0.027	24	
5333.65	[Fe II]	19F	5333.47	0.015	0.010	:	
5342.38	C II	17.06	5342.05	0.018	0.012	:	
5412.00	[Fe III]	1F	5411.95	0.037	0.023	26	
5423.20	N I		5422.86	0.009	0.006	:	g
5432.77	S II	6	5432.54	0.022	0.013	37	
5453.81	S II	6	5453.69	0.027	0.016	32	
5495.70	N II	29 }	5495.43	0.013	0.008	53	
5495.82	[Fe II]	17F }					
5506.87	[Cr III]		5506.52	0.008	0.004	:	
5512.77	O I	25	5512.60	0.029	0.014	31	
5517.71	[Cl III]	1F	5517.42	0.727	0.359	5	
5537.88	[Cl III]	1F	5537.60	0.807	0.396	5	
5542.58	S I		5542.41	0.015	0.007	:	g
5545.00	N I	29 }	5544.89	0.020	0.010	39	
5545.15	N I	29 }					
5551.95	N II	63	5551.63	0.012	0.006	:	g
5555.03	O I	24	5554.79	0.022	0.011	37	
5577.34	[O I]	3F	—	—	—	—	c
5581.86	[Fe II]	15F	5581.50	0.015	0.007	:	g
5666.64	N II	3	5666.32	0.045	0.021	23	
5676.02	N II	3	5675.68	0.030	0.014	30	
5679.56	N II	3	5679.29	0.084	0.039	15	

Table 2—Continued

λ_0 (Å)	Ion	Mult.	λ (Å)	$F(\lambda)^a$	$I(\lambda)^b$	Err(%)	notes
5686.21	N II	3	5685.90	0.011	0.005	:	
5710.76	N II	3	5710.52	0.011	0.005	:	
5754.64	[N II]	3F	5754.36	0.887	0.404	5	
5875.64	He I	11	5875.34	26.060	11.373	4	
5907.21	C II	44	5906.96	0.025	0.011	34	
5927.82	N II	28	5927.48	0.021	0.009	38	
5931.79	N II	28	5931.47	0.047	0.020	22	
5940.24	N II	28	5939.89	0.014	0.006	:	
5941.68	N II	28	5941.29	0.034	0.015	27	
5957.56	Si II	4	5957.29	0.053	0.023	21	
5958.58	O I	23	5958.40	0.095	0.040	14	
5978.93	Si II	4	5978.67	0.105	0.044	13	
6000.20	[Ni III]	2F	5999.94	0.016	0.007	:	
6046.44	O I	22	6046.19	0.095	0.039	14	
6151.43	C II	16.04	6151.17	0.030	0.012	30	
6300.30	[O I]	1F	6300.05	1.515	0.570	5	c
6312.10	[S III]	3F	6311.73	4.122	1.544	5	
6347.11	Si II	2	6346.77	0.387	0.143	7	
6363.78	[O I]	1F	6363.53	0.556	0.205	6	c
6371.36	Si II	2	6371.00	0.353	0.129	8	
6454.80	C II	17.05F	6454.54	0.011	0.004	:	
6462.00	C II	17.04	6461.53	0.090	0.032	15	
6527.10	[N II]	1F	6526.87	0.021	0.007	38	
6548.03	[N II]	1F	6547.76	35.114	12.107	5	
6562.21	H I	H3	6562.43	768.576	263.627	5	
6578.05	C II	2	6577.64	0.731	0.249	6	
6583.41	[N II]	1F	6583.12	112.131	38.183	5	
6666.80	[Ni II]	2F	6666.53	0.019	0.006	:	
6678.15	He I	46	6677.76	10.897	3.589	6	
6716.47	[S II]	2F	6716.12	17.940	5.830	6	
6721.39	O II	4	6720.92	0.011	0.004	27	
6730.85	[S II]	2F	6730.50	22.585	7.302	6	
6733.90	[Cr IV]	$^4F-^2G$	6733.62	0.012	0.004	26	g
6739.80	[Fe IV]	$^2G-^2I$	6739.75	0.020	0.006	18	
6744.39	C II		6744.08	0.015	0.005	22	
6747.50	[Cr IV]	$^4F-^2G$	6747.21	0.012	0.004	26	
6755.90	He I	1/20	6755.49	0.013	0.004	24	g
6769.61	N I		6769.22	0.014	0.004	23	g
6785.81	O II		6785.37	0.012	0.004	26	e, g
6791.25	Ne II		6790.94	0.015	0.005	22	g
6813.57	[Ni II]	8F	6813.27	0.008	0.003	33	
6818.22	N II		6817.97	0.008	0.003	33	g
6855.88	He I	1/12					e
7002.23	O I	21	7001.82	0.213	0.067	7	c
7062.26	He I	1/11	7062.04	0.074	0.023	9	
7065.28	He I	10	7064.82	19.453	5.919	6	

Table 2—Continued

λ_0 (Å)	Ion	Mult.	λ (Å)	$F(\lambda)^a$	$I(\lambda)^b$	Err(%)	notes
7083.00	Ar I		7082.70	0.035	0.010	13	g
7110.90	[Cr IV]		7110.59	0.017	0.005	20	
7113.42	Si II		7112.87	0.013	0.004	24	g
7115.40	Si I		7115.13	0.011	0.003	28	g
7135.78	[Ar III]	1F	7135.36	53.072	15.581	6	
7155.14	[Fe II]	14F	7154.83	0.126	0.036	8	
7160.58	He I	1/10	7160.13	0.069	0.020	10	
7231.12	C II	3	7230.84	0.332	0.093	7	
7236.19	C II	3	7235.94	0.531	0.148	7	
7237.17	C II	3	7236.80	0.067	0.019	10	
7254.38	O I	20	7254.21	0.134	0.037	8	
7281.35	He I	45	7280.92	2.447	0.669	7	
7298.05	He I	1/9	7297.61	0.104	0.028	9	
7318.39	[O II]	2F	7318.63	2.358	0.633	7	
7319.99	[O II]	2F	7319.74	9.400	2.522	7	
7329.66	[O II]	2F	7329.31	5.540	1.479	7	c
7330.73	[O II]	2F	7330.38	5.078	1.355	7	
7377.83	[Ni II]	2F	7377.53	0.202	0.053	8	
7388.17	[Fe II]	14F	7387.75	0.021	0.006	18	
7390.60	[Cr IV]	1F	7390.38	0.029	0.007	15	
7411.61	[Ni II]	2F	7411.34	0.051	0.013	11	
7423.64	N I	3	7423.29	0.054	0.014	11	
7442.30	N I	3	7442.01	0.109	0.028	9	
7452.54	[Fe II]	14F	7452.20	0.049	0.012	12	
7468.31	N I	3	7467.99	0.168	0.042	8	
7477.10	Si I		7476.56	0.012	0.003	26	g
7499.18	He I	1/8	7499.43	0.177	0.044	8	
7504.94	O II		7504.51	0.015	0.004	22	
	?		7512.83	0.034	0.008	14	
7519.86	Si I		7519.42	0.019	0.005	20	
7530.54	[Cl IV]	1F	7529.96	0.032	0.008	14	
7538.06	Si I		7537.56	0.008	0.002	35	g
7714.54	He I	2/15	7714.04	0.020	0.005	19	
7751.10	[Ar III]	2F	7750.68	17.582	3.894	8	c
7771.94	O I	1	7771.38	0.051	0.011	12	c
7774.17	O I	1	7773.66	0.254	0.056	8	c
7816.13	He I	1/7	7815.68	0.321	0.069	8	
7837.76	Ar II		7837.42	0.012	0.003	26	g
7875.99	[P II]		7875.46	0.038	0.008	14	g
7971.62	He I	2/11	7971.08	0.041	0.008	13	
8000.08	[Cr II]	1F	7999.56	0.074	0.015	11	
8030.69	Ar II		8030.31	0.022	0.004	18	g
8045.63	[Cl IV]	1F	8045.24	0.075	0.015	11	
8057.	He I	4/18	8057.07	0.030	0.006	16	
8084.	He I	4/17	8083.78	0.034	0.007	15	
8094.08	He I	2/10	8093.85	0.193	0.037	9	

Table 2—Continued

λ_0 (Å)	Ion	Mult.	λ (Å)	$F(\lambda)^a$	$I(\lambda)^b$	Err(%)	notes
8116.	He I	4/16	8115.91	0.041	0.008	13	
8125.30	[Cr II]	1F	8124.91	0.033	0.006	15	d
8184.85	N I	2	8184.53	0.098	0.018	10	d
8188.01	N I	2	8187.65	0.191	0.036	14	d
8200.91	C II		8200.	—	—		c
8203.85	He I	4/14	8203.35	0.071	0.013	11	
8210.72	N I	2	8210.34	0.052	0.010	12	
8216.28	N I	2	8215.96	0.236	0.044	9	
8245.64	H I	P42	8245.13	0.212	0.039	9	
8247.73	H I	P41	8247.27	0.215	0.039	9	
8249.20	H I	P40	8249.48	0.222	0.041	9	
8252.40	H I	P39	8251.90	0.263	0.048	9	
8255.02	H I	P38	8254.55	0.306	0.056	9	
8257.85	H I	P37	8257.45	0.228	0.042	9	
8260.93	H I	P36	8260.52	0.279	0.051	9	
8264.28	H I	P35	8263.92	0.351	0.064	9	
8265.71	He I	4/13 } 2/9 }	8265.29	0.088	0.016	11	
8267.94	H I	P34	8267.46	0.395	0.072	9	
8271.93	H I	P33	8271.40	0.423	0.077	9	
8276.31	H I	P32	8275.83	0.450	0.082	9	
8281.12	H I	P31	8280.50	0.376	0.068	9	c, d
8286.43	H I	P30	8285.86	0.441	0.080	9	
8292.31	H I	P29	8291.78	0.652	0.118	9	
8298.83	H I	P28	8298.22	0.492	0.089	9	
8306.11	H I	P27	8305.77	0.432	0.078	9	
8314.26	H I	P26	8313.75	0.683	0.122	9	
8323.42	H I	P25	8322.94	0.792	0.141	9	
8333.78	H I	P24	8333.29	0.856	0.152	9	
8342.33	He I	4/12	8341.85	0.111	0.020	10	
8359.00	H I	P22	8358.51	1.125	0.198	9	
8361.67	He I	1/6	8361.22	0.624	0.110	9	
8374.48	H I	P21	8373.98	1.134	0.199	9	
8376.	He I	6/20	8375.95	0.068	0.012	11	
8388.00	Ar I		8387.35	0.024	0.004	18	g
8392.40	H I	P20	8391.89	1.459	0.254	9	
8397.	He I	6/19	8396.86	0.057	0.010	12	
8413.32	H I	P19	8412.82	1.644	0.284	9	
8422.	He I	6/18	8421.45	0.062	0.011	12	
8424.	He I	7/18	8423.91	0.039	0.007	14	
8433.85	[Cl III]	3F	8432.99	0.048	0.008	13	g
8437.96	H I	P18	8437.46	1.892	0.325	9	
8444.34	He I	4/11 } 267 }	8444.00	0.161	0.028	10	c
8444.34	N III						
8446.48	O I	4	8446.12	3.725	0.638	9	c
8451.00	He I	6/17	8450.70	0.080	0.014	11	
8467.25	H I	P17	8466.76	2.194	0.373	9	
8480.90	[Cl III]	3F	8480.36	0.049	0.008	13	

Table 2—Continued

λ_0 (Å)	Ion	Mult.	λ (Å)	$F(\lambda)^a$	$I(\lambda)^b$	Err(%)	notes
8486.	He I	6/16	8485.80	0.102	0.017	10	
8488.	He I	7/16	8488.26	0.040	0.007	14	
8500.00	[Cl III]	3F	8499.35	0.104	0.018	10	
8502.48	H I	P16	8501.98	2.690	0.452	9	
8518.04	He I	2/8	8517.52	0.070	0.012	11	
8528.99	He I	6/15	8528.54	0.136	0.023	10	
8531.48	He I	7/15	8531.08	0.051	0.009	13	
8665.02	H I	P13	8664.48	5.302	0.847	9	
8680.28	N I	1	8680.07	0.265	0.042	10	
8683.40	N I	1	8683.02	0.179	0.028	10	
8686.15	N I	1	8685.87	0.183	0.029	10	
8703.25	N I	1	8702.87	0.123	0.019	10	
8711.70	N I	1	8711.32	0.144	0.023	10	
8718.84	N I	1	8718.46	0.075	0.012	12	
8727.13	[C I]	3F	8726.85	0.162	0.025	10	c
8728.90	[Fe III]	8F	8728.76	0.063	0.010	12	
8728.90	N I	28					
8733.43	He I	6/12	8732.92	0.239	0.037	10	
8736.04	He I	7/12	8735.51	0.078	0.012	11	
8737.83	Ar II		8737.80	0.016	0.003	23	g
8739.97	He I	5/12	8739.54	0.023	0.004	18	
8750.47	H I	P12	8749.96	7.051	1.098	9	
8776.77	He I	4/9	8776.44	1.185	0.183	9	
8816.82	He I	10/12	8816.13	0.044	0.007	14	
8829.40	[S III]	3F	8829.14	0.088	0.013	11	
8845.38	He I	6/11	8844.94	0.401	0.061	10	
8848.05	He I	7/11	8847.43	0.110	0.017	11	
8854.11	He I	5/11?	8853.59	0.047	0.007	13	
8862.26	H I	P11	8862.26	9.615	1.449	10	
8891.91	[Fe II]	13F	8891.51	0.079	0.012	12	
8894.21	O II		8893.46	0.033	0.005	16	g
8914.77	He I	2/7	8914.22	0.152	0.023	10	
8930.97	He I	10/11	8930.11	0.047	0.007	14	
8996.99	He I	6/10	8996.45	0.485	0.070	10	
8999.40	He I	7/10	8999.16	0.142	0.021	11	
9014.91	H I	P10	9014.39	13.007	1.571	11	d
9063.29	He I	4/8	9062.71	0.302	0.036	11	
9068.90	[S III]	1F	9068.39	272.159	32.644	11	
9085.13	He I	10/10	9084.81	0.083	0.010	12	
9095.10	Ar II		9094.68	0.080	0.010	12	g
9123.60	[Cl II]		9123.17	0.212	0.025	11	
9204.17	O II		9203.65	0.108	0.013	12	
9210.28	He I	6/9	9209.79	0.676	0.080	11	
9213.20	He I	7/9	9212.59	0.187	0.022	11	
9229.01	H I	P9	9228.45	18.038	2.120	11	d
9303.42	He I	10/9	9302.86	0.187	0.022	11	d
9463.57	He I	1/5	9463.10	1.096	0.125	11	

Table 2—Continued

λ_0 (Å)	Ion	Mult.	λ (Å)	$F(\lambda)^a$	$I(\lambda)^b$	Err(%)	notes
9516.57	He I	4/7	9515.93	0.585	0.066	11	d
9526.16	He I	6/8	9526.09	0.910	0.103	11	
9530.60	[S III]	1F	9530.42	709.953	80.424	11	d
	?		9537.38	0.239	0.027	11	d
9545.97	H I	P8	9545.47	17.376	1.965	11	d
9603.44	He I	2/6	9602.81	0.256	0.029	11	
	?		9822.48	0.029	0.003	18	
9824.13	[C I]		9823.77	0.287	0.031	11	
9850.26	[C I]		9849.93	0.861	0.094	11	
9903.46	C II	17.02	9902.88	0.738	0.080	11	
10027.70	He I	6/7	10027.12	2.065	0.221	11	
10031.20	He I	7/7	10030.55	0.735	0.079	11	
10049.37	H I	P7	10048.79	54.885	5.853	11	
10138.42	He I	10/7	10137.81	0.283	0.030	12	
10286.73	[S II]	3F	10286.08	1.084	0.113	11	
10310.70	He I	4/6	10310.37	2.796	0.290	11	c
10320.49	[S II]	3F	10319.93	3.016	0.312	11	
10336.41	[S II]	3F	10335.85	2.528	0.261	11	
10340.83	O I		10340.39	0.531	0.055	11	
10370.50	[S II]	3F	10369.95	1.114	0.115	11	

^aWhere F is the observed flux in units of $100.00 = 1.056 \times 10^{-12}$ ergs cm⁻² s⁻¹.

^bWhere I is the reddened corrected flux, with $C(H\beta)=1.40$ dex, in units of $100.00 = 2.653 \times 10^{-11}$ ergs cm⁻² s⁻¹.

^cAffected by telluric emission lines.

^dAffected by atmospheric absorption bands.

^eAffected by internal reflections or charge transfer in the CCD.

^fBlend with an unknown line.

^gDubious identification.

Table 3. Physical Conditions.

Diagnostic	Line	
N_e (cm^{-3})	[O II] ($\lambda 3726$)/($\lambda 3729$)	950 ± 100
	[O II] ($\lambda 3726 + \lambda 3729$)/($\lambda 7320 + \lambda 7330$)	$2300 \pm 200^{\text{a}}$
	[S II] ($\lambda 6716$)/($\lambda 6731$)	1300^{+500}_{-300}
	[Fe III]	3200 ± 400
	[Cl III] ($\lambda 5518$)/($\lambda 5538$)	3500^{+900}_{-700}
	[Ar IV] ($\lambda 4711$)/($\lambda 4740$)	4500^{+2600}_{-1800}
	Adopted value	2800 ± 400
T_e (K)	[N II] ($\lambda 6548 + \lambda 6583$)/($\lambda 5755$)	$8500 \pm 200^{\text{a}}$
	[S II] ($\lambda 6716 + \lambda 6731$)/($\lambda 4069 + \lambda 4076$)	8400^{+350}_{-600}
	[O III] ($\lambda 4959 + \lambda 5007$)/($\lambda 4363$)	8500 ± 50
	[Ar III] ($\lambda 7136 + \lambda 7751$)/($\lambda 5192$)	8600^{+450}_{-350}
	[S III] ($\lambda 9069 + \lambda 9532$)/($\lambda 6312$)	9300^{+500}_{-400}
	Adopted value	8500 ± 150
	He II	6800 ± 400
	Balmer decrement	6650 ± 750
	Paschen decrement	6700 ± 900

^aRecombination contribution to the intensity of the auroral lines subtracted (see text).

Table 4. t^2 parameter.

Method	t^2
O ⁺⁺ (R/C)	0.038 ± 0.006
Ne ⁺⁺ (R/C)	$0.036^{+0.014}_{-0.024}$
FL–Pac	$0.038^{+0.013}_{-0.019}$
FL–Bac	0.036 ± 0.017
Adopted	0.038 ± 0.009

Table 5. He^+/H^+ ratios from singlet lines.

$\lambda_0(\text{\AA})$	He^+/H^+	$12+\log(\text{He}^+/\text{H}^+)$
5015.47	0.0827 ± 0.0013	10.92
3964.50	0.0919 ± 0.0031	10.96
3613.42	0.0935 ± 0.0081	10.97
6677.76	0.0804 ± 0.0045	10.91
4921.69	0.0836 ± 0.0014	10.92
4387.67	0.0877 ± 0.0023	10.94
4009.01	0.0769 ± 0.0050	10.89
4143.52	0.0830 ± 0.0037	10.92
4437.29	0.1160 ± 0.0114	11.06
7280.92	0.1049 ± 0.0089	11.02
Adopted	0.0866 ± 0.0080	10.94 ± 0.04

Table 6. Ionic abundances from collisional excited lines^a.

X^m	$t^2=0.000$	$t^2=0.038\pm0.009$
N^+	7.09 ± 0.06	7.25 ± 0.06
O^+	8.15 ± 0.07	8.32 ± 0.07
O^{++}	8.35 ± 0.03	8.63 ± 0.08
Ne^{++}	7.61 ± 0.09	7.91 ± 0.10
S^+	5.75 ± 0.08	5.91 ± 0.08
S^{++}	6.99 ± 0.10	7.30 ± 0.10
Cl^+	4.13 ± 0.08	4.26 ± 0.08
Cl^{++}	4.95 ± 0.06	$5.21^{+0.09}_{-0.07}$
Cl^{3+}	3.21 ± 0.07	3.42 ± 0.08
Ar^{++}	6.34 ± 0.05	6.57 ± 0.08
Ar^{3+}	4.20 ± 0.07	4.48 ± 0.09
Fe^{++}	5.57 ± 0.05	5.85 ± 0.09
Fe^{3+}	$5.71^{+0.17}_{-0.29}$	$5.95^{+0.12}_{-0.16}$

^aIn units of $12+\log(\text{X}^m/\text{H}^+)$.

Table 7. C^{++}/H^+ ratio from C II lines.

Mult	λ (Å)	$I(\lambda)/I(\text{H}\beta)$	$\text{C}^{++}/\text{H}^+ (\times 10^{-5})$	
		$[I(\text{H}\beta)=100]$	A	B
2	6578.05 ^a	0.224	269	46
3	7231.12	0.093	2408	34
	7236.19	0.148	2176	31
	Average		2266	32
	$m_{\text{cf}}=1.09$			
	Sum	0.257	2260	32
6	4267.26	0.295	27	27
16.04	6151.43	0.012	27	26
17.02	9903.46	0.080	29	–
17.04	6462.00	0.032	28	–
17.06	5342.38	0.012:	20	–
Adopted			28 ± 4	

^aAffected by a telluric emission line.

Table 8. Nitrogen abundances from permitted lines^a.

ion	Mult	λ (Å)	$I(\lambda)/I(\text{H}\beta)$	$X^{+i}/\text{H}^+ (\times 10^{-5})$		notes
			$[I(\text{H}\beta)=100]$	A	B	
N^+	1	8680.28	0.042	117	114	
		8683.40	0.028	151	147	
		8686.15	0.029	393	381	
		8703.25	0.019	241	234	
		8711.70	0.023	237	230	
		8718.84	0.012	152	147	
		Average		212	205	
	2	$m_{\text{cf}}=1.02$				
		Sum		175	170	
		8184.85	0.018	281	239	
		8188.01	0.036	570	484	
		8210.72	0.010	389	331	
		8216.28	0.044	266	226	
		Average		381	323	
	3	$m_{\text{cf}}=1.48$				
		Sum		339	288	
		7423.64	0.014	1360	444	
		7442.30	0.028	1348	440	
		7468.31	0.042	1353	441	
		Average		1353	441	
		$m_{\text{cf}}=1.00$				
		Sum		1353	441	
N^{++}	3	5666.64	0.021	12	10	KS02
		5676.02	0.014	18	15	
		5679.56	0.039	12	10	
		5686.21	0.005:	8	7	
		5710.76	0.005:	8	7	
		Average		13	11	
		$m_{\text{cf}}=1.07$				
	5	Sum		12	10	KS02
		4601.48	0.013	107	18	
		4613.87	0.010	188	32	
		4621.39	0.023	272	46	
		4630.54	0.055	144	24	
		4643.06	0.027	212	36	
		Average		181	30	
	20	$m_{\text{cf}}=1.12$				KS02
		Sum		164	28	
		4803.29	0.019	1195	23	
		4779.71	0.009	1615	23	
		4788.13	0.017	1957	38	
		Average		1573	31	
		$m_{\text{cf}}=1.27$				
	28	Sum		1498	29	KS02
		5927.82	0.009	2629	31	

Table 8—Continued

ion	Mult	λ (Å)	$I(\lambda)/I(\text{H}\beta)$	$X^{+i}/\text{H}^+ (\times 10^{-5})$		notes
			$[I(\text{H}\beta)=100]$	A	B	
		5931.79	0.020	2568	30	
		5940.24	0.006:	2240	26	
		5941.68	0.015	1017	12	
		Average		2059	24	
		$m_{\text{cf}}=1.10$				
		Sum		1703	20	
	48	4239.4	0.034	8	8	EV90
Adopted				10 ± 1		

^aOnly lines with intensity uncertainties lower than 40% have been considered.

^bRecombination coefficients from: KS02 = Kisieliu & Storey (2002), EV90 = Escalante & Victor (1990).

Table 9. O^+/H^+ ratio from O I lines.

Mult	λ (Å)	$I(\lambda)/I(\text{H}\beta)$	$\text{O}^+/\text{H}^+ (\times 10^{-5})^{\text{a}}$	
		$[I(\text{H}\beta)=100]$	A	B
1	7771.94	0.011	11/15	–
	7774.17 ^b	0.056	80/103	–
4	8446.48 ^b	0.638	2425/3641	548/730
Adopted			13 ± 3	

Table 10. O^{++}/H^+ ratio from O II lines^a.

Mult	λ (Å)	$I(\lambda)/I(H\beta)$ [$I(H\beta)=100$]	O^{++}/H^+ ($\times 10^{-5}$)		
			A	B	C
1	4638.85	0.074	73	70	–
	4641.81	0.132	47	45	–
	4649.14	0.145	29	28	–
	4650.84	0.069	70	68	–
	4661.64	0.090	72	69	–
	4673.73	0.013	84	81	–
	4676.23	0.040	43	41	–
	4696.36	0.007:	79	76	–
	Average		53	51	–
	$m_{cf}=1.00$				
2	Sum		46	45	–
	4317.14	0.026	48	35	–
	4319.63	0.019	37	26	–
	4345.56 ^b	0.057	103	73	–
	4349.43	0.067	48	34	–
	4366.89	0.040	63	45	–
	Average		51	36	–
	$m_{cf}=1.28$				
4	Sum		49	35	–
	6721.39	0.004:	60	–	47
	$m_{cf}=1.50$				
	Sum		60	–	47
5	4414.90	0.029	56	–	9
	4416.97	0.031	108	–	17
	Average		82	–	13
	$m_{cf}=1.07$				
10 ^c	Sum		74	–	12
	4069.62				
	4069.89	0.139	54/52	–	–
	4072.15	0.085	35/34	–	–
	4075.86	0.108	30/30	–	–
	4085.11	0.024	47/53	–	–
-	Average		42/41	–	–
	$m_{cf}=1.10/1.25$				
	Sum		39/ 39	–	–
	15 ^d				
15 ^d	4590.97	0.029	164	–	–
	4595.95				
	4596.18	0.010	190	–	–
	Average		176	–	–
	$m_{cf}=1.00$				
19 ^c	Sum		176	–	–
	4129.32	0.009:	4647/2219	175/135	175/126
	4132.80	0.035	1560/1181	59/61	59/57
	4153.30	0.043	1419/1240	54/54	54/50
	4156.54 ^f	0.028	6744/4005	255/219	255/205
	Average		1482/1214	56/57	56/54
	$m_{cf}=1.37/1.47$				

Table 10—Continued

Mult	λ (Å)	$I(\lambda)/I(\text{H}\beta)$ [$I(\text{H}\beta)=100$]	$\text{O}^{++}/\text{H}^+ (\times 10^{-5})$		
			A	B	C
20 ^c	Sum		1481/1215	56/ 57	56/53
	4110.78	0.015	195/455	190/60	190/57
	4119.22	0.023	13/26	12/25	12/13
	Average		85/196	83/39	83/31
	$m_{\text{cf}}=2.42/1.89$				
25 ^c	Sum		20/41	19/ 33	19/19
	4699.21	0.007:	100/105	100/91	5/9
	4705.35	0.008:	77/69	77/67	4/4
	Average		88/86	88/79	4/7
	$m_{\text{cf}}=1.03/1.04$				
3d–4f ^e	Sum		87/82	87/77	4/5
	4083.90	0.017	–	52	–
	4087.15	0.026	–	81	–
	4089.29	0.044	–	37	–
	4275.55	0.019	–	30	–
	4285.69	0.015	–	66	–
	4332.71	0.013:	–	116	–
	4491.23 ^b	0.022	–	137	–
	4602.13	0.006:	–	28	–
	4609.44	0.024	–	48	–
	Average		–	50	–
	Adopted		42 ± 5		

Table 11. $\text{Ne}^{++}/\text{H}^+$ ratio from Ne II lines.

Mult	λ (Å)	$I(\lambda)/I(\text{H}\beta)$ [$I(\text{H}\beta)=100$]	$\text{Ne}^{++}/\text{H}^+ (\times 10^{-6})$	
			A	B
55e	4391.99	0.018:	55	–
	4409.30	0.024:	111	–
	Average		87	–
	$m_{\text{cf}}=1.00$			
	Sum	0.042	77	–
Adopted			77 ± 25^a	

Table 12. Total gaseous abundances^a.

Element	$t^2=0.000$	$t^2=0.038$
He	10.97 ± 0.03	10.97 ± 0.04
C ^b	8.47 ± 0.06	8.46 ± 0.06
N	7.63 ± 0.06	7.87 ± 0.07
N ^c	—	8.07 ± 0.08
O	8.56 ± 0.03	8.80 ± 0.07
O ^b	8.74 ± 0.06	8.74 ± 0.06
Ne	7.82 ± 0.10	8.09 ± 0.12
Ne ^b	8.09 ± 0.10	8.07 ± 0.11
S	7.05 ± 0.10	7.36 ± 0.10
Cl	5.02 ± 0.06	5.26 ± 0.08
Ar	6.38 ± 0.06	6.61 ± 0.08
Fe ^d	$5.96^{+0.09}_{-0.11}$	6.30 ± 0.14
Fe ^e	$5.95^{+0.11}_{-0.15}$	6.20 ± 0.12

^aIn units of $12+\log(X/H)$.

^bFrom recombination lines (RLs).

^c N^+/H^+ from collisional excited lines (CELs) and N^{++}/H^+ from permitted lines.

^dAssuming $ICF(Fe)$.

^e $Fe/H = Fe^{++}/H^+ + Fe^{3+}/H^+$.

Table 13. Comparison of NGC 3576 gaseous abundance determinations^a.

Element	This work ($t^2=0.00$)	(1)	(2)	(3)	(4)
	$\alpha=11:12:0.9$ $\delta=-61:18:19.1$	$\alpha=11:12:0.5$ $\delta=-61:18:24$	$\alpha=11:14:50.1.4$ $\delta=-61:37:35.3$	$\alpha=11:12:48.1$ $\delta=-61:33:12.3$	$\alpha=11:11:46.6$ $\delta=-61:18:43$
He ⁺	10.97	10.97	10.94	10.98	—
C ^{++b}	8.47	8.46	—	—	—
N ⁺	7.09	7.07	7.45	7.20	—
N ⁺⁺	8.00 ^c	8.43 ^c	—	—	7.68
N	7.63 ^d	7.55 ^d	7.58	7.56	7.85
O ⁺	8.15	8.04	8.55	8.18	—
O ^{+b}	8.11	—	—	—	—
O ⁺⁺	8.35	8.34	8.08	8.30	8.43
O ^{+++b}	8.62	8.57	—	—	—
O ^e	8.56	8.52	8.67	8.55	—
Ne ⁺⁺	7.61	7.54	7.16	7.35	7.70
Ne	7.82	7.72	7.75	7.40	8.00
S ⁺	5.67	5.79	6.16	5.84	—
S ⁺⁺	6.99	—	6.82	6.80	6.86
S	7.05	≥ 5.82	7.03	7.49	7.04
Cl ^{+f}	4.13	—	—	—	—
Cl ⁺⁺	4.95	5.00	—	—	—
Cl ³⁺	3.21	—	—	—	—
Cl	5.02	5.18	—	—	—
Ar ⁺⁺	6.34	6.23	5.98	6.21	—
Ar ³⁺	4.20	4.33	—	—	—
Ar	6.38	6.41	—	—	—

^aREFERENCES.- (1) Tsamis et al. (2002); (2) (3) Girardi et al. (1997); (4) Simpson et al. (1995).

^bAbundances from RLs.

^cAbundances from permitted lines probably affected by fluorescence.

^d*ICF* assumed.

^eOnly from CELs.

^fAtomic data not reliable (see text).

Table 14. NGC 3576 and Solar abundances^a.

Element	NGC 3576	Sun ^c	NGC 3576–Sun
He	10.97±0.04	10.98±0.02	−0.01
C ^b	8.56±0.06	8.41±0.05	+0.15
N	7.86±0.07	7.80±0.05	+0.06
O ^b	8.82±0.06	8.66±0.05	+0.16
Ne	8.08±0.12	7.84±0.06	+0.24
S	7.36±0.10	7.20±0.08	+0.16
Cl	5.26±0.08	5.28±0.08	−0.02
Ar	6.61±0.08	6.18±0.08	+0.43
Fe	7.66±0.20	7.50±0.05	+0.16

^aIn units of 12+log(X/H).

^bValues derived from RLs.

^cChristensen-Dalsgaard (1998); Grevesse & Sauval (1998); Asplund (2003); Asplund et al. (2004).

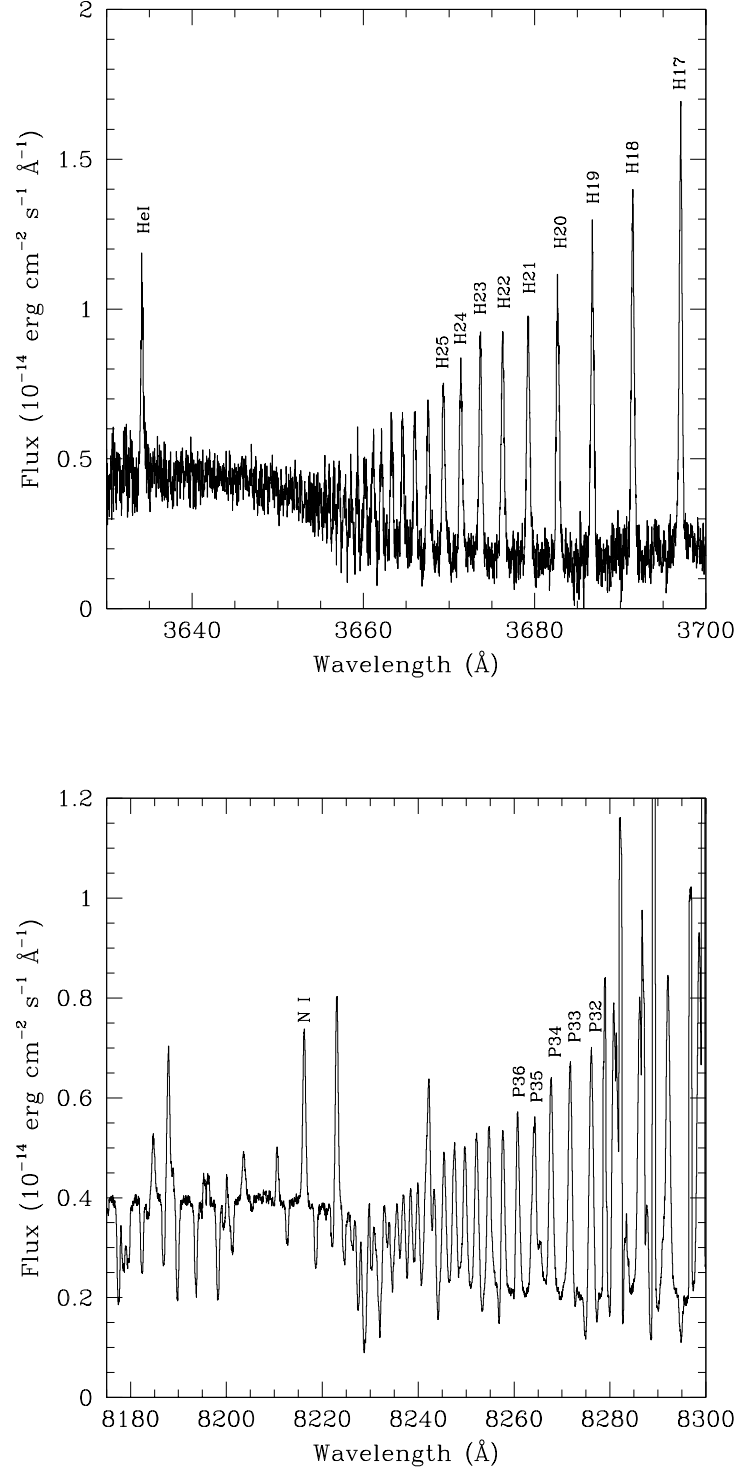


Fig. 1.— Section of the echelle spectrum including the Balmer (top) and the Paschen (bottom) limits (observed fluxes).

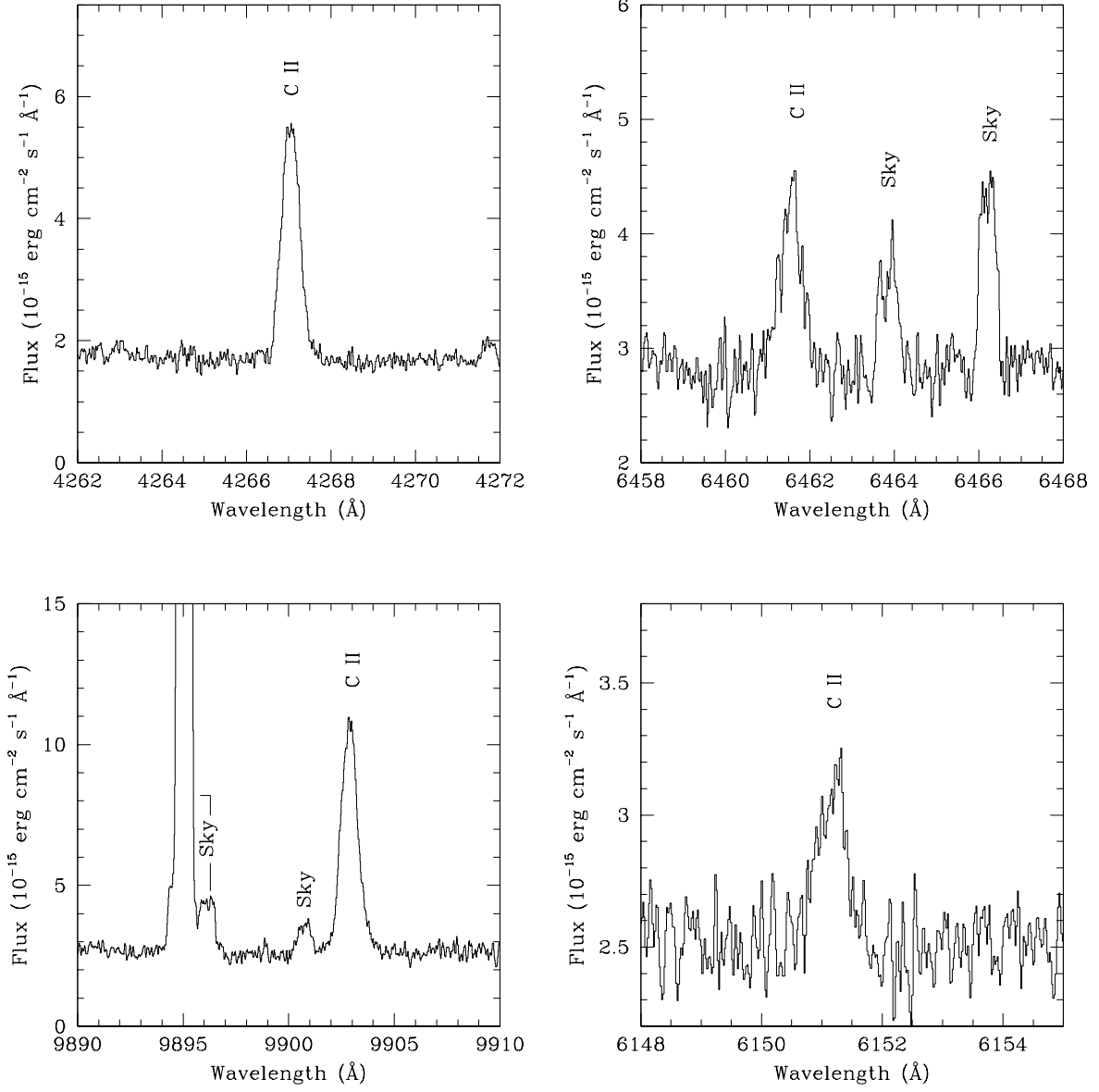


Fig. 2.— Sections of the echelle spectrum of NGC 3576 showing the brightest lines of C II detected

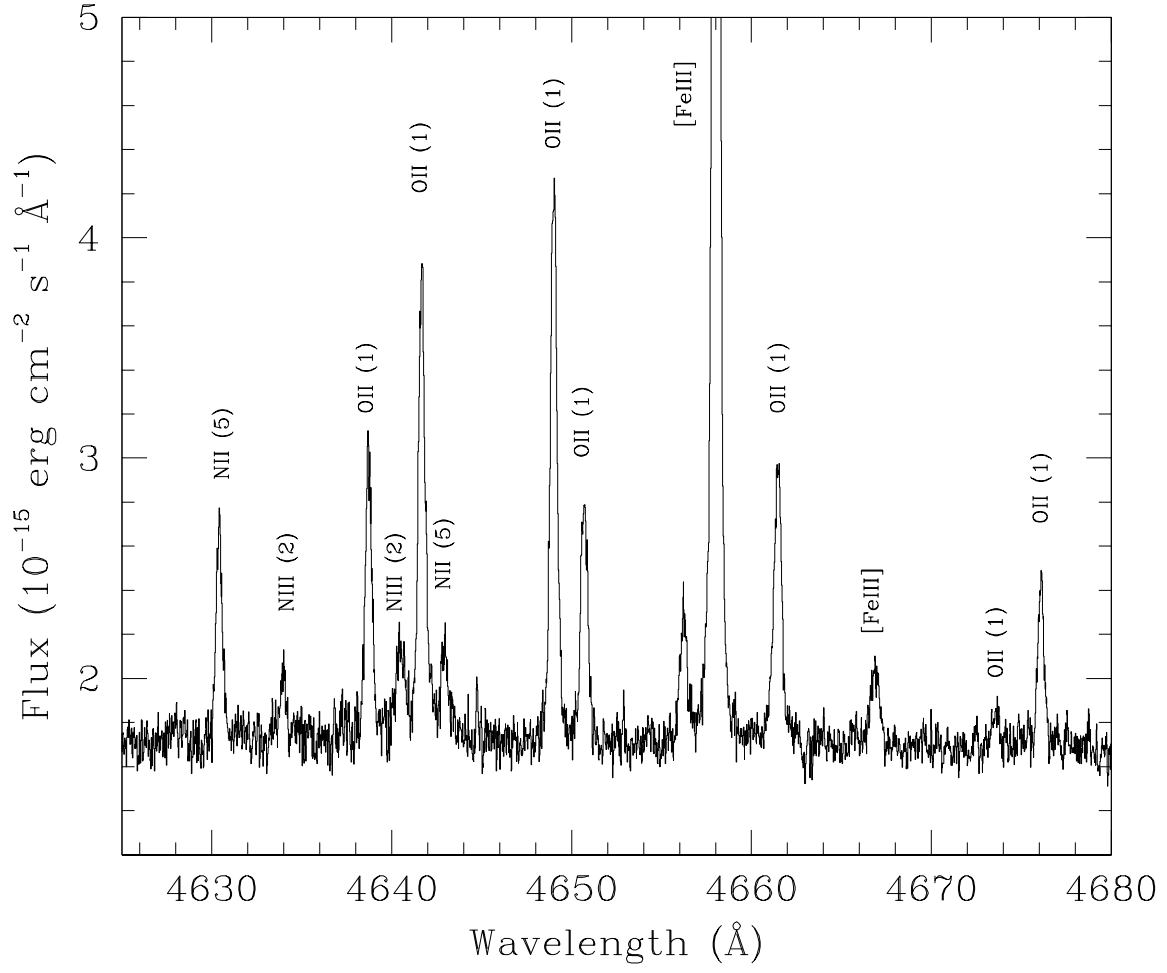


Fig. 3.— Section of the echelle spectrum of NGC 3576 showing all the lines of multiplet 1 of O II.

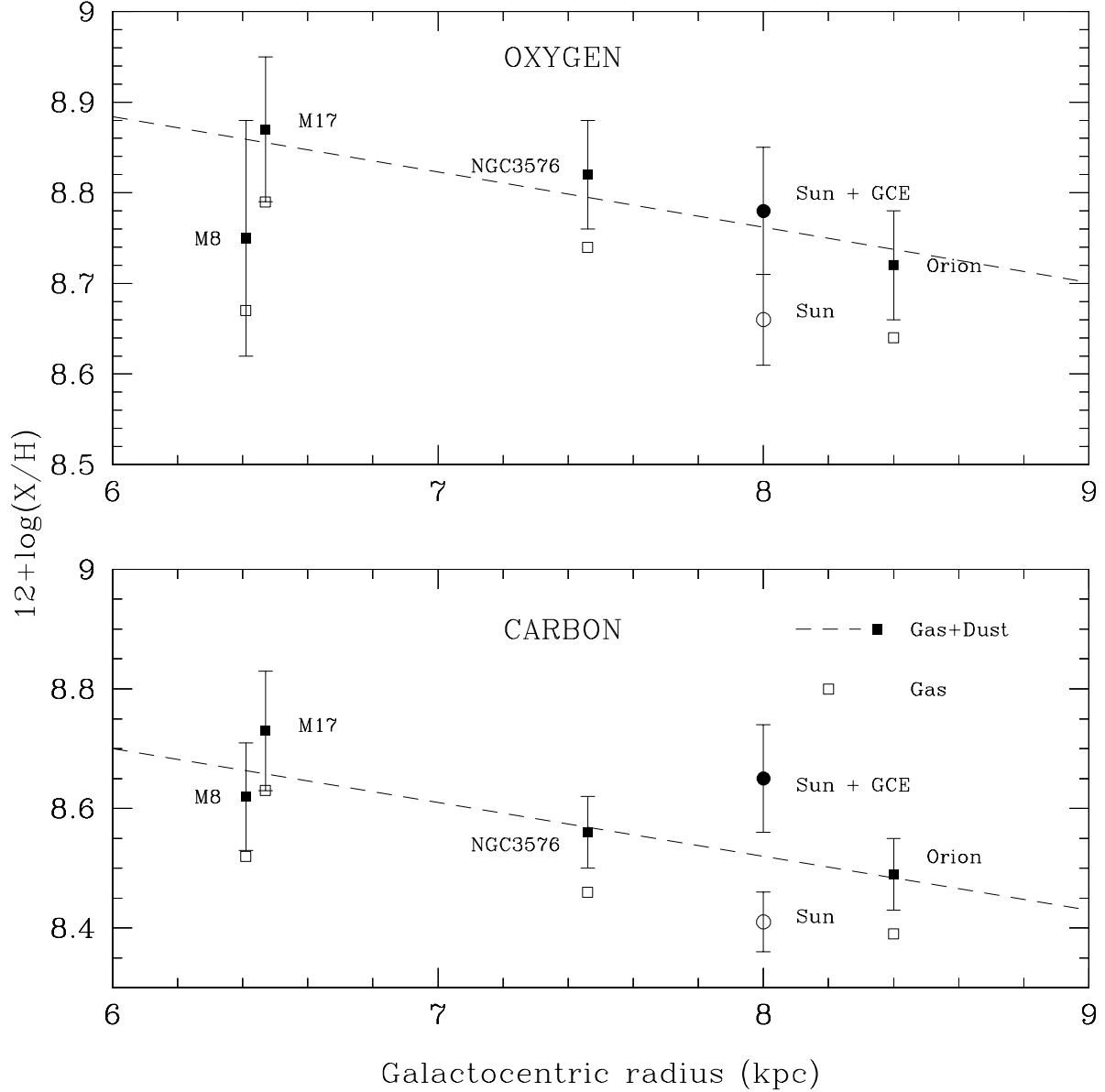


Fig. 4.— Galactic O and C radial abundance gradients from H II region abundances determined from recombination lines. Filled squares are dust+gas abundances, derived applying the corrections proposed by EPTE. Open squares are the gas-phase abundances. Both sets of data have similar error bars, which are only indicated for the filled squares. Abundance data for the Orion nebula, M8 and M17 have been taken from EPTE, EPTGR and Esteban et al. (1999b), respectively. Galactocentric distances have been taken from Russeil (2003). Open circles are the Solar abundances given by Asplund (2003); Asplund et al. (2004). Filled circles are the values expected for the interstellar medium at the solar Galactocentric distance, based on the solar values and models for Galactic chemical evolution, GCE (Carigi 2003; Akerman et al. 2004). The broken lines represent the correlation found for the H II regions dust+gas abundances.